HIGHWAY RESEARCH RECORD

Number 167

Bridges and Structures

5 Reports

Subject Area
27 Bridge Design

HIGHWAY RESEARCH BOARD
DIVISION OF ENGINEERING NATIONAL RESEARCH COUNCIL
NATIONAL ACADEMY OF SCIENCES—NATIONAL ACADEMY OF ENGINEERING

Washington, D.C., 1967 Publication 1447

Department of Design

W. B. Drake, Chairman
Assistant State Highway Engineer for Planning, Research and Materials
Kentucky Department of Highways, Lexington

HIGHWAY RESEARCH BOARD STAFF

L. F. Spaine, Engineer of Design

BRIDGE DIVISION

J. N. Clary, Chairman
Bridge Engineer
Virginia Department of Highways, Richmond

COMMITTEE ON STEEL SUPERSTRUCTURES
(As of December 31, 1966)

Arthur L. Elliott, Chairman
Bridge Engineer—Planning
California Division of Highways, Sacramento

John W. Fisher, Research Assistant Professor, Fritz Laboratory, Lehigh University, Bethlehem, Pennsylvania
Carl H. Gronquist, Partner, Steinman, Boynton, Gronquist and London, New York, New York
T. R. Higgins, Director of Engineering and Research, American Institute of Steel Construction, New York, New York
William H. Munse, Jr., Department of Civil Engineering, University of Illinois, Urbana
Sidney L. Poleynard, Bridge Design Engineer, Louisiana Department of Highways, Baton Rouge
A. A. Toprac, Professor of Civil Engineering, University of Texas, Austin
Ivan M. Viest, Structural Engineer, Sales Engineering Division, Bethlehem Steel Corporation, Bethlehem, Pennsylvania

COMMITTEE ON SUBSTRUCTURES, RETAINING WALLS AND FOUNDATIONS
(As of December 31, 1966)

Wayne Henneberger, Chairman
Engineer of Bridge Design, Texas
Highway Department, Austin

Raymond Archibald, Otis, Oregon
F. M. Fuller, Assistant Vice President, Raymond International, Inc., New York, New York
H. D. Gibbons, The Union Metal Manufacturing Company, Canton, Ohio
T. J. Hirsch, Associate Professor of Civil Engineering, and Associate Research Engineer, Texas Transportation Institute, Texas A & M University, College Station
W. T. Hunzicker, Assistant Bridge Engineer, Arizona Highway Department, Phoenix
Joseph H. Moore, Head, Civil Engineering Department, Clemson University, Clemson, South Carolina
Joe S. Robinson, Chief Engineer, Delaware State Highway Department, Dover
Charles B. Trueblood, Armco Steel Corporation, Armco Division, Middletown, Ohio

Foreword

The five papers contained in this RECORD are directed to a variety of subjects of interest to those involved in research, design and construction of highway structures.

The first paper summarizes the results of a research project on the behavior of longitudinally stiffened plate girders subjected to pure bending and to high shear. In both loading cases, Cooper found that substantial increase in strength was achieved through the use of longitudinal stiffeners. The study was limited to static strength of symmetrical members. The requirements for proportioning and positioning of the stiffeners are also discussed.

Fatigue strength of hybrid plate girders under constant moment was studied by Lew and Toprac. The objects of the research were to determine the manner in which thin web hybrid-girders fail when subjected to repeated loads and to determine what factors influence the fatigue strength of this type of girder. The results led to the conclusion that fatigue cracks occurred within 2 million cycles if the applied stress exceeded the yield point of the web material. Web flexing action and fluctuating membrane stresses were the factors found to cause fatigue failure in the web. Specimens were tested at several stress levels and ranges.

In the third paper a computer program for the analysis of folded plate structures of general form was used to study the lateral distribution of load in simple span composite box girder bridges without transverse diaphragms or internal stiffeners. Johnston and Mattock used the results to develop simple expressions for the loads carried by the interior and exterior girders in this type of bridge. The accuracy of the analysis was confirmed by the results of a quarter-scale model of a two-lane, 80-foot span bridge supported by three box girders.

The need for a low-cost rapidly erected short-span bridge unit has resulted in the development of a conceptual design for a prefabricated composite unit consisting of a concrete deck connected by horizontal studs to two inverted steel T-beams. McDermott presents in this paper design curves and details for spans from 30 feet to 80 feet. He concludes that such a bridge unit is both structurally adequate and economical.

The final paper presents an abridgment of a study to determine the bearing capacity of piles by dynamic methods. Recent developments in electronic instrumentation make it possible to record acceleration and force near the top of a pile. Goble, Scanlan and Tomko present a theory relating these dynamic measurements to static capacity. Good correlation was found to exist between static capacity as determined by load tests and static capacity as determined by the proposed theory.

Contents

The Contribution of Longitudinal Stiffeners To the Static Strength of Plate Girders

PETER B. COOPER, Research Assistant, Lehigh University

This paper summarizes the results of a research project on the behavior of longitudinally stiffened plate girders subjected to either pure bending or high shear. Analytical and experimental studies were conducted to determine the increase in the static strength of plate girders due to the presence of longitudinal stiffeners. Requirements for positioning and proportioning longitudinal stiffeners are also discussed.

•THE provisions in the AASHO specifications (1) for determining the proportions of a plate girder web and the location and size of web stiffeners are primarily based on stability considerations, i.e., the theoretical web buckling stress is the criterion for failure or limit of usefulness. However, because of a redistribution of stress in the web and the supporting action of the flanges and stiffeners which frame the web, the maximum load which a girder can sustain is considerably higher than the theoretical web buckling load (2). In many cases where plate girder design is based on web buckling theory, the existence of post-buckling strength is tacitly recognized by the use of a low factor of safety against web buckling (3).

In this paper the type of stress redistribution which occurs in a plate girder web is discussed for the separate loading cases of pure bending and high shear. In particular, the effect of a longitudinal stiffener on the stress redistribution is described for these two loading cases.

When investigating the influence of longitudinal stiffeners on the behavior of plate girders, it is helpful first to study the behavior of transversely stiffened plate girders (2, 4, 5). Based on this information and observations of the behavior of longitudinally stiffened test girders, the effect of longitudinal stiffeners can then be explored.

BENDING STRENGTH

The behavior of transversely stiffened plate girders subjected to pure bending can be described using the test data on lateral web deflections and bending stresses shown in Figure 1. Shown in Figure 1a are the web deflection patterns measured at three different test loads. The web deflections increased continuously in the upper half of the girder, which was subjected to compressive bending stresses. There is no indication of a sudden change in the magnitude of the deflections such as would be expected according to web buckling theory.

Another illustration is provided by the curves of bending stress distribution (Fig. 1b). The dark lines represent the measured stresses and the light lines represent the linear stress distributions computed from conventional beam theory ($\sigma = My/I$). In the lower portion of the web, the measured tensile stresses correspond very closely to those predicted by beam theory; however, due to the increasing lateral web deflections in the compression zone, a redistribution of compressive stresses from the web to the compression flange occurs. The stresses in a significant portion of the web between the neutral axis and the compression flange are essentially zero; the compression flange and a portion of the web adjacent to it carry stresses which exceed those predicted by beam theory.

Paper sponsored by Committee on Steel Superstructures and presented at the 46th Annual Meeting.

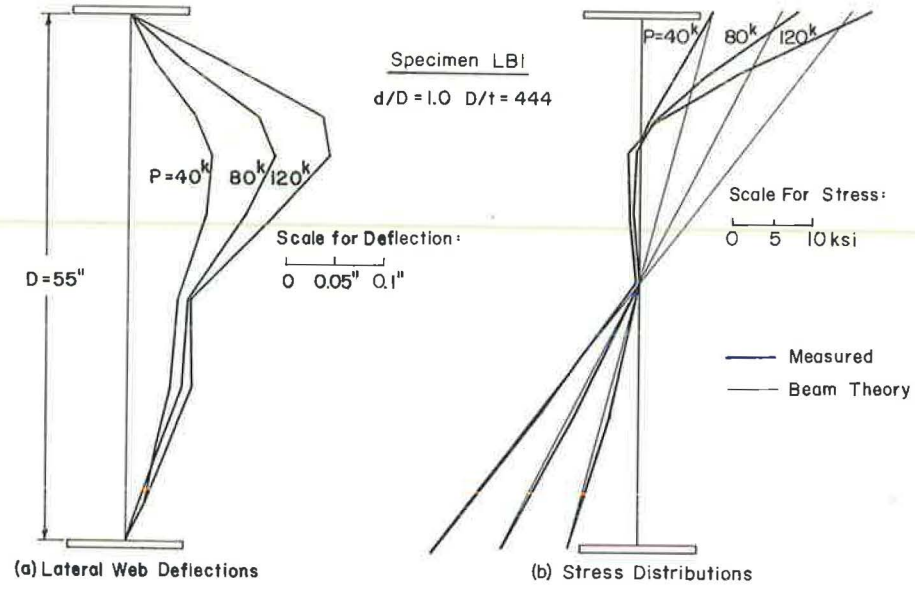

Figure 1. Test measurements on a transversely stiffened girder.

A flange stress reduction formula has been adopted for transversely stiffened girders to compensate for the increase in compression flange stress above the beam theory stress due to the stress redistribution (4). The magnitude of reduction is a function of the web slenderness ratio since the extent of the stress redistribution increases with higher slenderness ratios.

A longitudinal stiffener placed in the zone between the neutral axis and the compression flange reduces or completely eliminates lateral web deflections and thus has a significant effect on the stress redistribution described. This effect is illustrated by the web deflection and bending stress distribution data (Fig. 2). The test girder in Figure 2 was essentially identical to that in Figure 1, except for the presence of a longitudinal stiffener located $\frac{1}{5}$ of the web depth from the compression flange. Because of the presence of the longitudinal stiffener, the extent of the increase in lateral web deflections shown in Figure 2a is substantially smaller than that shown for a transversely stiffened girder (Fig. 1a).

Further information on the influence of longitudinal stiffeners on bending strength can be obtained from a comparison of the stress distributions in Figures 1b and 2b. Although the initial web deflections of the longitudinally stiffened specimen caused the bending stresses in the web to deviate somewhat from the linear beam theory distribution (Fig. 2b), a redistribution of stress from the web to the compression flange of the type shown in Figure 1b is not evident. Beam theory could be used to predict accurately the compression flange stresses for the longitudinally stiffened girder.

From this discussion it may be concluded that if a suitably positioned and proportioned longitudinal stiffener is used, beam theory can be used to predict the compression flange stresses. In this case a flange stress reduction is not necessary. Thus, by preserving the beam-type action the longitudinal stiffener will have a significant and beneficial effect on the bending strength. The percentage increase in the bending strength due to the longitudinal stiffener is shown in Figure 3 as a function of the web slenderness ratio and the ratio of the area of the web to the area of the flange, A_w/A_f. For the practical range of A_w/A_f between 0. 5 and 2 and with a web slenderness ratio of 400, the increase in bending strength varies from about 6 percent to 30 percent.

A longitudinal stiffener should be located $\frac{1}{5}$ of the web depth from the compression flange to be effective in controlling the stress redistribution under pure bending (6).

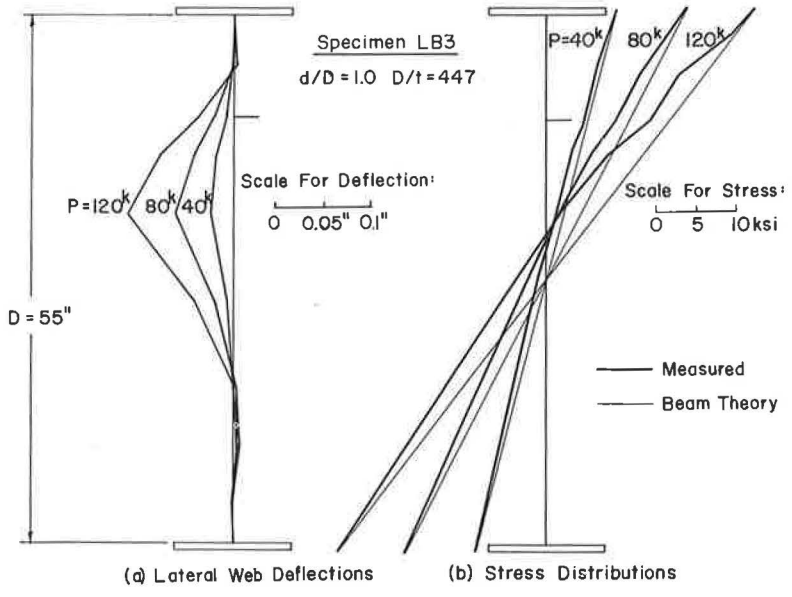

Figure 2. Test measurements on a longitudinally stiffened girder.

This is the position specified in the AASHO specifications (1). Requirements for proportioning longitudinal stiffeners are discussed in a separate section of this paper.

The bending strength theory described in this paper has been checked with the results of tests included in this program and tests conducted by others (6). The web slenderness ratios of the test girders ranged from 299 to 407. The ratios of the experimentally obtained ultimate loads to the ultimate loads predicted by the theory varied from 0. 94 to 1. 02 with a mean value of 0. 98. Due to the presence of the longitudinal stiffeners, the ultimate loads of these test girders were increased from 14 percent to 26 percent. The correlation of the bending strength theory with the test results is shown in Figure 4. Bar graphs are used for the ratio of the predicted ultimate load

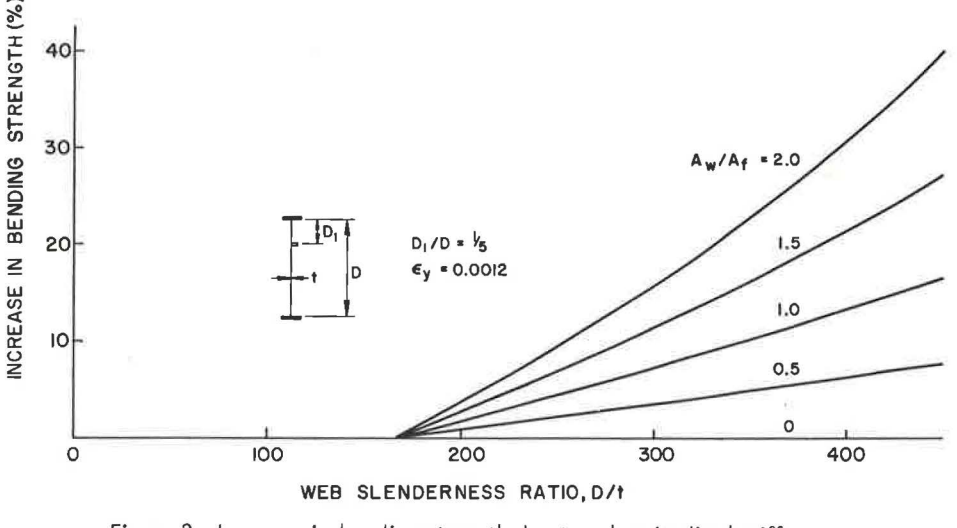

Figure 3. Increase in bending strength due to a longitudinal stiffener.

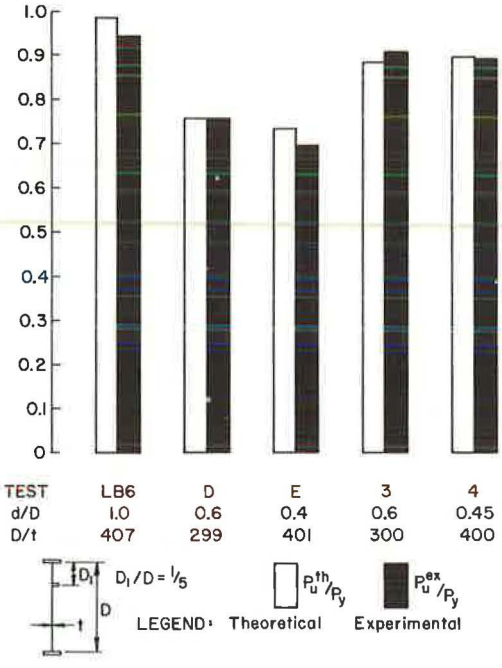

Figure 4. Correlation of bending strength theory with test results.

P_u^{th} to the yield load P_y and the ratio of the experimentally obtained ultimate load P_u^{ex} to the yield load. The test results indicate that a substantial increase in bending strength can be achieved by using longitudinal stiffeners, and that the theory provides a reliable estimate of the actual bending strength of longitudinally stiffened plate girders.

SHEAR STRENGTH

The type of shear panel which will be considered in this section is shown in Figure 5. The panel consists of a rectangular portion of the web bounded by the flanges and transverse stiffeners. It is assumed that the moment present on any section in the panel is small so that the shear strength of the panel can be studied independently.

An element subjected to pure shear stresses τ is shown in Figure 6a. These stresses correspond to the principal stresses shown in Figure 6b, where the tensile principal stress σ_1 is numerically equal to both the compressive principal stress σ_2 and the shear stress τ. The state of stress shown in Figure 6a is the type usually assumed in simple beam theory; in the following discussion it will be referred to as "beam action shear." As the shear force on a plate girder panel is increased, a stage is reached where the compressive stress σ_2 can no longer increase as rapidly as the tensile stress σ_1 because the web deflects laterally. For an ideal panel which is initially perfectly plane, this stage starts when the shear force reaches the critical value predicted by plate buckling theory. The stress in the direction of the tension diagonal continues to increase as the applied shear force increases beyond the critical shear force. A field of tensile stresses of the type shown in Figure 6b develops, and it is the source of the post-buckling shear strength of the panel. This state of stress is termed "tension field action shear."

Evidence of stress redistribution from the beam action type to the tension field action type in a plate girder web is shown in Figure 7—a photograph of a longitudinally stiffened test girder after it has been subjected to the ultimate shear force (7). The diagonal yield line patterns indicate the development of separate tension fields in the subpanels formed by the longitudinal stiffener.

Based on observations of test girders and the shear strength theory developed by Basler (5), the tension field model shown in Figure 8 has been used to estimate the shear strength of longitudinally stiffened plate girders (6). The following assumptions were used:

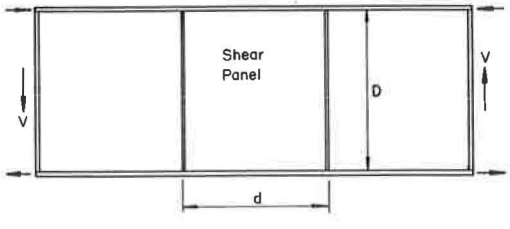

Figure 5. Typical shear panel.

1. The ultimate shear strength of a longitudinally stiffened panel is the sum of the shear strengths of the two subpanels;
2. The shear strength of a subpanel is the sum of the beam action contribution and the tension field action contribution;
3. The beam action contribution is the shear force carried by the web at the theoretical web buckling stress;

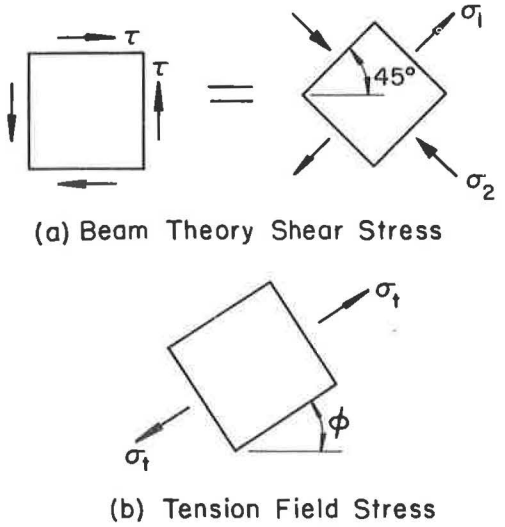

Figure 6. Stress states in a plate girder web.

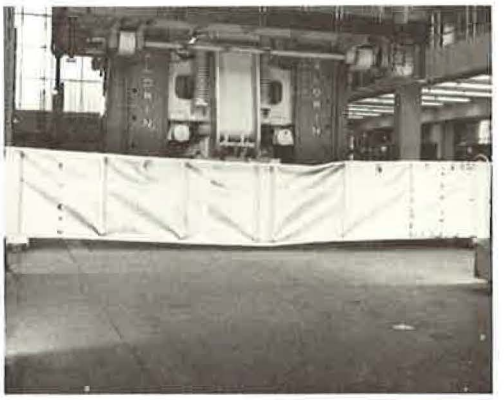

Figure 7. Longitudinally stiffened test girder after shear test.

4. The tension field contribution is the vertical component of the tension field force (Fig. 8); and
5. The ultimate subpanel shear forces will be reached when the combination of beam action and tension field action stresses cause yielding in the web.

The ultimate shear force of a longitudinally stiffened panel V_u, non-dimensionalized by the plastic shear force (the product of the web area and the yield stress in shear), is plotted against the web slenderness ration D/t for constant values of yield strain ϵ_y and aspect ratio d/D (Fig. 9). Curves are shown in the figure for three different longitudinal stiffener positions, illustrating that the stiffener position which provides the highest shear strength varies with the web slenderness ratio. The optimum longitudinal stiffener position moves from mid-depth toward the compression flange as the web slenderness ratio increases.

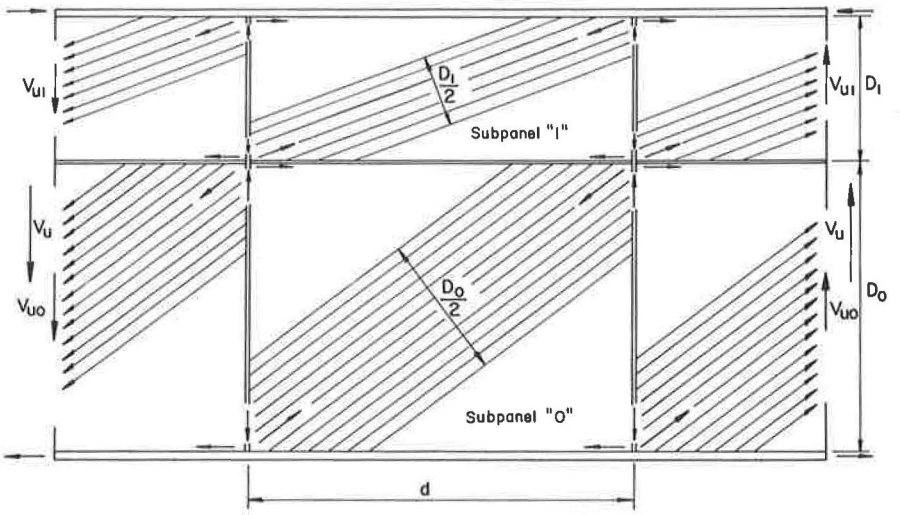

Figure 8. Tension field model for a longitudinally stiffened panel.

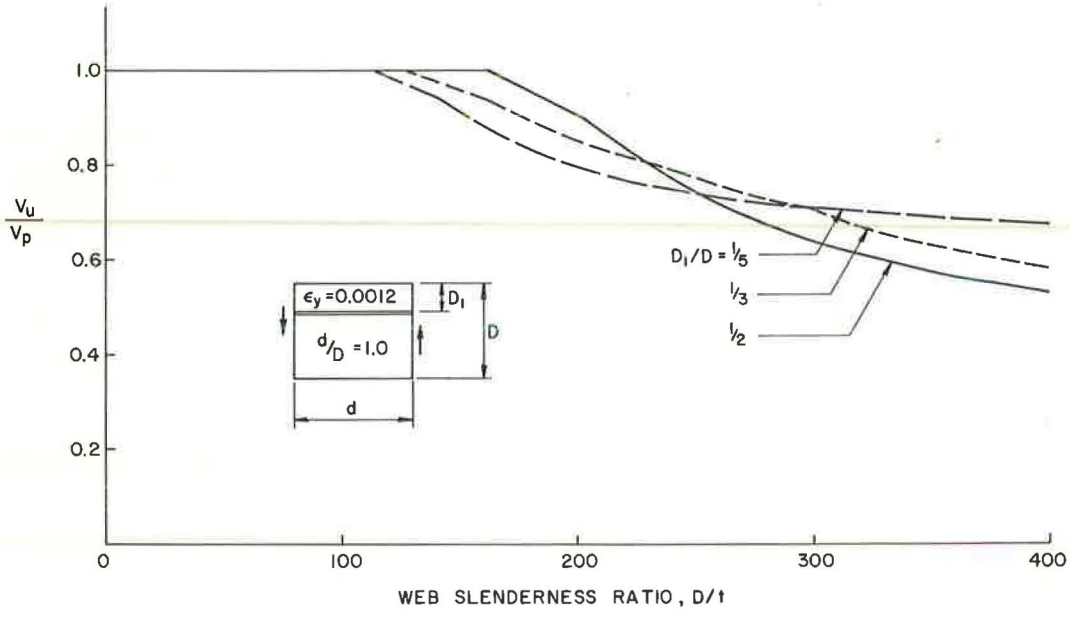

Figure 9. Shear strength curves for d/D = 1.0.

Using the optimum longitudinal stiffener position, the increase in the shear strength of a plate girder panel due to the use of a longitudinal stiffener is shown in Figure 10 as a function of the web slenderness ratio. The yield strain and aspect ratio are constants in this figure and have the same values as those used in Figure 9. According to the theory, the maximum increase in shear strength is about 26 percent for a slenderness ratio of about 160 with an increase of almost 10 percent for the entire range $120 \leq D/t \leq 400$ (Fig. 10). The increase in shear strength due to the longitudinal stiffener will be slightly different from that shown in Figure 10 for other values of yield strain and aspect ratio.

The results of seven longitudinally stiffened plate girder tests were used to check the shear strength theory described (6). In these tests three panel aspect ratios (d/D = 0. 75, 1. 0 and 1. 5) and three longitudinal stiffener positions ($D_1/D = 1/2$, $1/3$ and $1/5$) were used. The web slenderness ratio varied from 256 to 276. For the seven

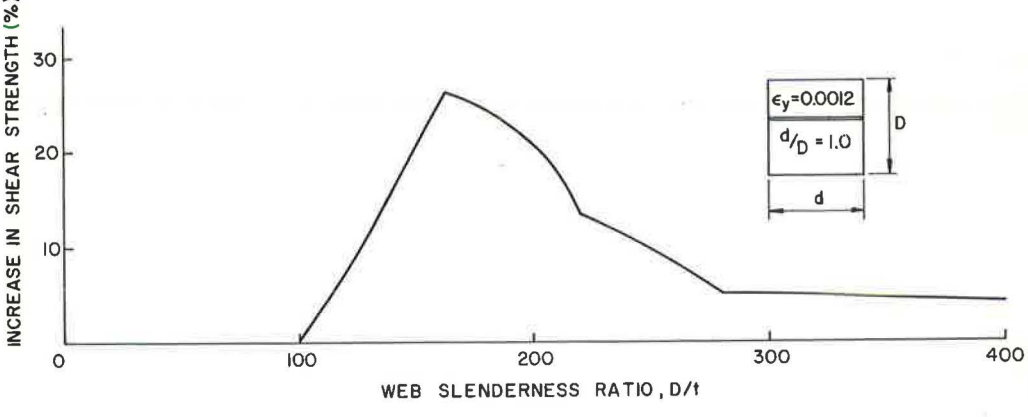

Figure 10. Increase in shear strength due to longitudinal stiffener.

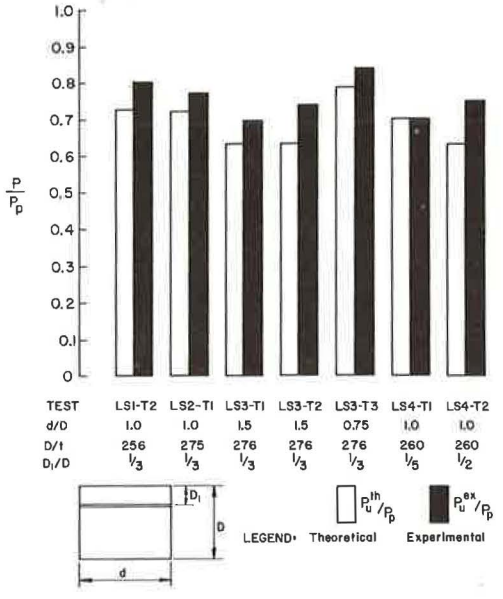

Figure 11. Correlation of shear strength theory with test results.

tests the ratio of the experimentally obtained ultimate loads P_u^{ex} to the ultimate loads predicted by the theory P_u^{th} ranged from 1.00 to 1.18 with a mean value of 1.10. The use of longitudinal stiffeners in the test specimens resulted in an increase in shear strength ranging from 6 percent to 38 percent. The ratios of P_u^{ex} and P_u^{th} to the plastic shear load P_p are shown in Figure 11 to provide a visual indication of the correlation of the shear strength theory with the seven test results. In summary, the test results indicate that the theory provides a reliable but somewhat conservative estimate of the actual shear strength of longitudinally stiffened plate girders and that the use of longitudinal stiffeners can lead to a substantial increase in shear strength.

LONGITUDINAL STIFFENER REQUIREMENTS

Three requirements are proposed for proportioning longitudinal stiffeners:

1. A minimum width-thickness ratio to prevent premature local buckling;
2. A minimum stiffener rigidity to force a nodal line in the deflected web; and
3. A minimum stiffener column strength to avoid premature lateral buckling.

The first requirement is the same for both bending and shear. Although the second requirement is intended to help insure that web deflections are controlled for both loading cases, for pure bending the purpose is to prevent a redistribution of stress from the web to the compression flange; for high shear the rigidity requirement is to insure that separate tension fields will form in the subpanels. Correspondingly, the numerical values of the minimum stiffener rigidity are different for the two loading cases (6). For the bending case, the compressive force used in checking the third requirement is that assigned to the stiffener section according to beam theory. In the case of high shear the minimum stiffener column strength is required to transfer the horizontal components of the tension fields from one side of a panel to the other (Fig. 8).

SUMMARY

Results of an investigation of the influence of longitudinal stiffeners on the behavior and strength of plate girders have been summarized. For the case of pure bending it was found that longitudinal stiffeners, by controlling lateral web deflections, help to maintain a linear bending stress distribution, thus eliminating the need for reduction in the flange stress. For a girder panel subjected to high shear, longitudinal stiffeners force the formation of separate tension fields in the subpanels. In both loading cases, a substantial increase in strength can be achieved by using longitudinal stiffeners.

Requirements for proportioning longitudinal stiffeners have been described. These requirements are applicable to both loading cases considered. The problem of positioning longitudinal stiffeners has also been treated for the two loading cases.

This study was limited to the static strength of symmetrical, longitudinally stiffened steel plate girders. Since longitudinal stiffeners are effective in controlling lateral web deflections, they should also have a beneficial effect on plate girder fatigue

strength. The effect of longitudinal stiffeners on the behavior and strength of unsymmetrical girders has not yet been determined. Research programs are in progress to investigate these related problems.

ACKNOWLEDGMENTS

This paper is based on research conducted at the Department of Civil Engineering, Fritz Engineering Laboratory, Lehigh University. The financial support provided by the Pennsylvania Department of Highways, the U. S. Bureau of Public Roads, the American Iron and Steel Institute and the Welding Research Council is gratefully acknowledged. The guidance of Alexis Ostapenko, director of the project, in preparing the manuscript is sincerely appreciated.

REFERENCES

1. AASHO. Standard Specifications for Highway Bridges. 8th Ed., 1961.
2. Basler, K., Yen, B. T., Mueller, J. A., and Thürlimann, B. Web Buckling Tests on Welded Plate Girders. Bull. 64, Welding Research Council, Sept. 1960.
3. Cooper, P. B. Plate Girders. Structural Steel Design, Chap. 8, Ronald Press, 1964.
4. Basler, K., and Thürlimann, B. Strength of Plate Girders in Bending. Trans. ASCE, Vol. 128, Part II, 1963.
5. Basler, K. Strength of Plate Girders in Shear. Trans. ASCE, Vol. 128, Part II, 1963.
6. Cooper, P. B. Static Strength of Longitudinally Stiffened Plate Girders. Fritz Engineering Laboratory Rept. 304.9, Lehigh University, June 1966. (To be published in Jour. Struct. Div. of ASCE.)
7. D'Apice, M. A., Fielding, D. J., and Cooper, P. B. Static Tests on Longitudinally Stiffened Plate Girders. Bull. 117, Welding Research Council, Oct. 1966.

Fatigue Strength of Hybrid Plate Girders Under Constant Moment

H. S. LEW, Research Engineer, and
A. A. TOPRAC, Professor of Civil Engineering, University of Texas

Two series of fatigue tests on welded hybrid plate girders are described. The first series consisted of 14 panel specimens and the second series consisted of 14 full-length specimens. In both series, the center test panel (or panels) was subjected to pure bending moment. The test specimens had ASTM A 514 steel flanges and ASTM A 36 steel webs. Flange dimensions were kept constant in all specimens, while web thicknesses used were $\frac{1}{8}$, $\frac{1}{16}$, $\frac{1}{4}$ and $\frac{3}{8}$ inch. To obtain an S-N curve the maximum bending stress in the flange was varied in both series along with the applied stress range.

The behavior of webs under repeated load are described, and fatigue cracks are discussed and their results are analyzed. It was observed that, regardless of the web thickness, webs moved laterally under load. The magnitudes of the lateral movement varied depending on the load and the shape of the initial crookedness of the web. Fatigue cracks were found both in the web and in the tension flange. Those found in web occurred along the toe of the compression flange-to-web fillet weld (Type 1) and near the end of the transverse stiffener (Type 2). Cracks developed in the tension flange (Type 3) were caused mainly by fabrication irregularities. In all cases the complete failure of a specimen was accompanied by a fracture through the tension flange.

•THE USE of high strength steels can result in significant savings in the cost of a structure because less weight of steel is required for high strength steel. Since the "weight-strength-price" ratio increases with strength, further savings can be made for flexural members by using high strength steel flanges in combination with lower strength steel web. Therefore, if the strength of the flange is to be fully utilized, the design of such a girder must then assume a yielded condition in the web adjacent to the flanges at working loads. Since initial yielding has been the design criterion for structural members of homogeneous cross section, an investigation of the behavior of such a yielded web is needed before a design method can be adopted for practical use.

The results of experimental studies have shown that straining the web beyond its yield point has little adverse effect on the static behavior of hybrid girders (1). However, insufficient information is available at present on the fatigue strength of such girders. Furthermore, whatever the findings in static tests which would allow the use of hybrid girders, the application of design rules to hybrid girders under repeated load can be justified only after the fatigue behavior has been fully investigated.

To establish design rules based on experimental work, a test program was planned to investigate full-size girders. The test specimens were subjected to various maximum stresses and stress ranges to obtain an S-N curve. In establishing the S-N

Paper sponsored by Committee on Steel Superstructures and presented at the 46th Annual Meeting.

curve, instead of attempting to establish a fatigue limit, i.e., to find the limiting value of the stress below which a girder can presumably endure an infinite number of stress cycles, this investigation was aimed at obtaining a finite life based on the number of cycles to crack initiation.

OBJECTIVES AND SCOPE

The objectives of this investigation were (a) to determine the manner in which slender web hybrid girders fail when subjected to pure bending fatigue loading, and (b) to determine the factors that influence the fatigue strength of this type of girder when subjected to cycles of constant stress. The stress levels, the minimum and maximum stresses, were selected so that each specimen of the same web thickness would be tested to a specific combination of minimum stress and stress range.

The specimens were subjected to at least 2 million cycles of repeated stress if no fractures appeared which caused an increase in deflection beyond the stroke capacity of the hydraulic jacks used for testing. The 2 million number was chosen because it was considered to be the largest number of cycles of maximum load conditions that any member in a bridge will ever experience during its useful life.

DESIGN CONSIDERATION

Previous investigations made on hybrid girders (2) indicated that if the web was too thin with respect to the depth of a girder, repeated loads caused fluctuating lateral deformations of the web, thereby inducing the development of fatigue cracks along the web boundaries. In order to study the effect of web thickness on the fatigue strength, all geometric configurations and cross-sectional dimensions of each girder test program were kept constant except the thickness of the web. Web slenderness ratio (the ratio of web depth to thickness) was adopted as the variable geometric parameter.

To vary the web slenderness ratio, different web thicknesses were selected from readily available structural steel plates. The selection was made so that two groups of the web slenderness ratio would be below and two above the ratio of 170 specified by the AASHO (3) bridge specifications for 33-ksi yield-point steel. The test program encompassed all practical ranges of ratios that would normally be encountered in bridge design. The ratios corresponding to the nominal web thicknesses of $^3/_8$, $^1/_4$, $^3/_{16}$ and $^1/_8$ in. for the chosen web depth of 36 in. were 86, 144, 192, and 288, respectively.

TEST PROGRAM AND TEST SPECIMENS

The test program was designed such that at least one specimen of each web thickness would be subjected to various maximum stress levels, namely, 20, 30, 40 and 50 ksi. The ranges of stress which were associated with the maximum stresses were chosen conveniently as 10, 15 and 25 ksi. To insure that sufficient yielding would occur in the web of a test specimen under the maximum stress, it was decided to use ASTM A 514 steel for the flanges and ASTM A 36 steel for the web.

The test specimens were divided into two groups, panel specimens (Series A) and full-length specimens (Series B). There were 14 specimens in each series. For both series, the flange dimensions were kept a constant 8 in. by $^1/_2$ in. A schematic array of the stress levels and the corresponding stress ranges for each test specimen is shown in Table 1, together with the nominal web slenderness ratios. Figure 1 shows loading arrangements for the two series.

BEHAVIOR OF WEB UNDER REPEATED LOAD

The amount of lateral movement of the web under the load is dependent on the magnitude and configuration of the initial deformation of the web. The magnitude of these initial deviations of the web from a plane surface may vary from girder to girder, and the shape of the initial deformation may differ from panel to panel of a girder, if an inconsistent order of placing the intermediate stiffener is used during the fabrication.

TABLE 1

STRESS LEVELS AND STRESS RANGES
FOR EACH TEST SPECIMEN

Specimen No.[a]		Nominal Web Thickness	Slenderness Ratio	Stress Levels		Stress Ranges (ksi)
Series A	Series B			Min	Max	
21020A	21020B	1/8 inch	288	10	20	10
21530A	21530B			15	30	15
21540A	21540B			15	40	25
22540A	22540B			25	40	15
22550A	22550B			25	50	25
None	31020B	3/16 inch	192	10	20	10
	31530B			15	30	15
	31540B			15	40	25
	32540B			25	40	15
	32550B			25	50	25
41020A	None	1/4 inch	144	10	20	10
41530A	41530B			15	30	15
41540A	41540B			15	40	25
42540A	42540B			25	40	15
42550A	42550B			25	50	25
61530A	None	3/8 inch	96	15	30	15
61540A				15	40	25
62540A				25	40	15
62550A				25	50	25

[a]The first digit represents the web thickness, while the last four digits show the minimum and maximum applied stress.

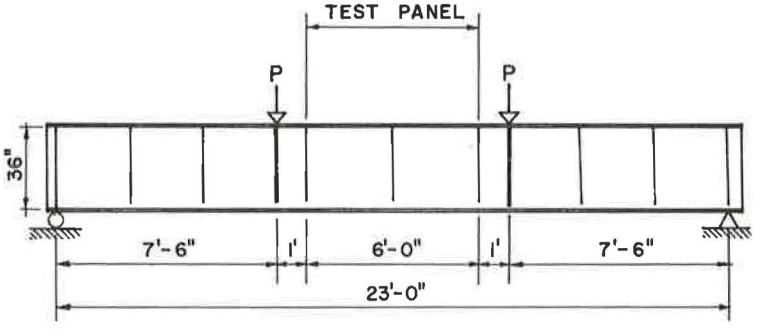

FULL LENGTH SPECIMEN

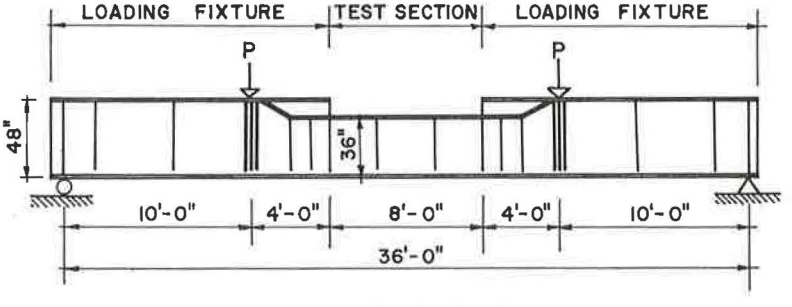

PANEL SPECIMEN

Figure 1. Test set-ups.

Measurements taken from each test specimen revealed that in most cases the slender webs had relatively larger initial deformations than the stockier webs. For example, most of the 1/8-in. web specimens had deformations greater than their web thicknesses (the maximum value observed was 1.88 times the web thickness), while the 3/8-in. web specimens had deformations about 0.25 times their web thicknesses.

The general trend observed on the shape of the initial web deformation was that in most cases the 1/8- and 3/16-in. specimens had either double or triple curvature, whereas the 1/4- and 3/8-in. specimens had single curvature. Typical examples of these cases are shown in Figures 2, 3, and 4 in contours and cross-sectional profile plots.

When the applied loads imposed bending moment on an initially crooked web panel, the part of the web under compressive flexural stress experienced an increase in deformation while the part under tensile flexural stress flattened toward a plane surface. Such a typical trend is shown in Figure 5, in which the cross-sectional profiles of a web panel are plotted at 3-in. intervals.

Based on the foregoing observations, the behavior of a web under repeated load can be summarized as follows. When the applied loads fluctuate between two load levels, thus imposing changing magnitude of pure bending moments on the initially distorted web panel, the portion of the web above the neutral axis moves in and out with an increased intensity in unison with the loads while the portion below the neutral axis moves in and out with a decreased intensity. As a result, the laterally deformed shape of a web cross section changes from one configuration to another as the magnitude of applied load changes. In Figure 6 such a change in cross-sectional shape is illustrated by plotting the web profiles of a panel at $P = 0$, P_{min} and P_{max}. The terms P_{min} and P_{max} refer respectively to the loads which cause the minimum and maximum stresses at the extreme fibre. The cross-hatched portion indicates the range of the web movements between P_{min} and P_{max}.

FATIGUE CRACKS

Three types of cracks were observed, categorized according to their locations with respect to the web panel. The Type 1 cracks were those found in the compression zone of the web along the toe of the flange-to-web fillet weld. The cracks always formed in the heat-affected zone of the web (Fig. 7).

The Type 2 cracks were those that started in the tension zone of web at the end of transverse stiffeners (Fig. 7). Except in a few cases in which the cracks began in the fillet weld itself, most cracks started in the heat-affected zone of the web.

The Type 3 cracks were those that occurred in the tension flange as a result of fabrication irregularities and the unfavorable geometry of the tension flange which induced local stress concentrations (Fig. 7).

Type 1 Cracks

The Type 1 cracks were found only in the 1/8-in. and 3/16-in. web specimens. These cracks were usually found in the center portion of a web panel and propagated in both directions, as shown in Figure 8. Since the development of such a crack is related to the web flexing action, in all cases the crack started in the convex side of the web where the surface was subjected to tensile stress due to bending of the web. Figure 9 illustrates this phenomenon.

The significant fact observed during the testing was that the rate of increase in length of Type 1 cracks was usually small and, furthermore, these cracks had a negligible effect on the overall stiffness of a girder.

Type 2 Cracks

Irrespective of the web thickness, Type 2 cracks were found in all groups of test specimens. This indicates that in the development of a Type 2 crack, the longitudinal bending stress coupled with a local stress concentration due to the abrupt termination of transverse stiffener was the major cause of crack initiation rather than local flexural stress due to the web flexing action as noted in the Type 1 cracks.

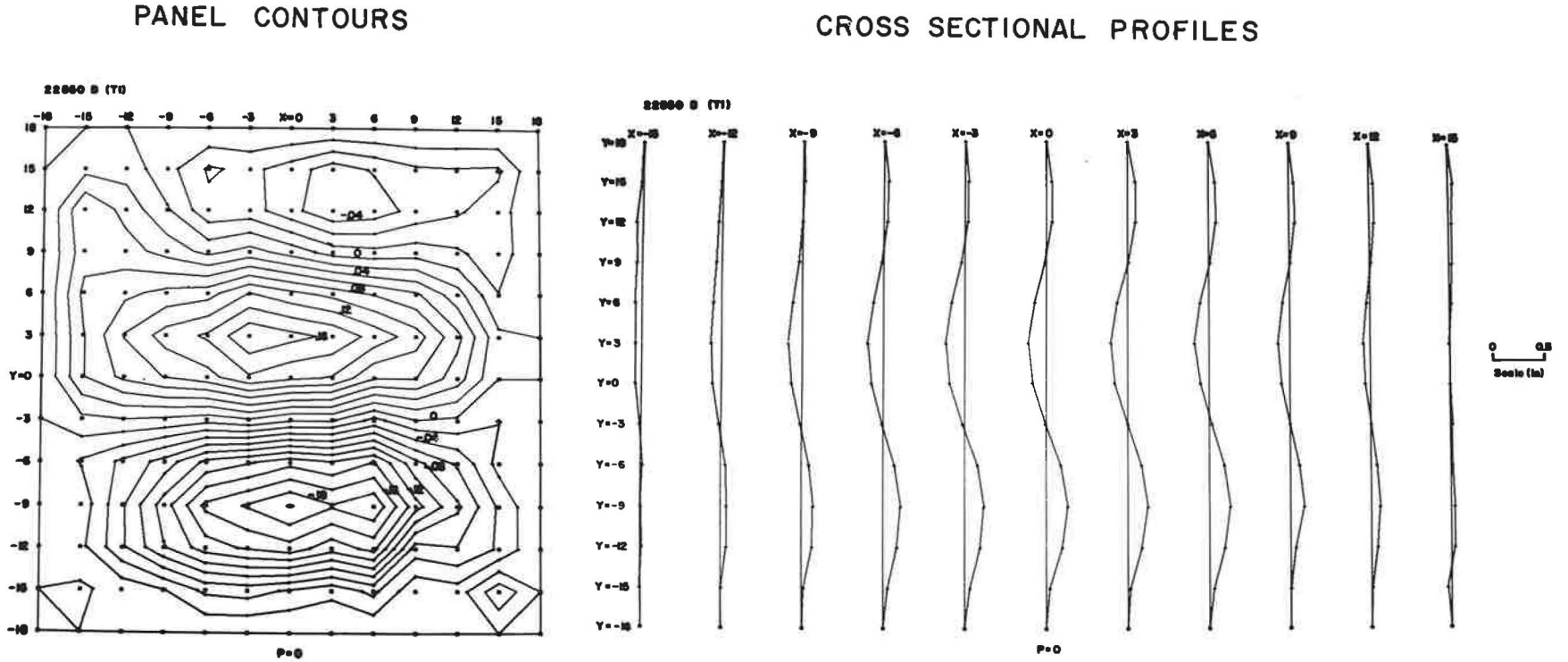

Figure 2. Triple curvature initial deformation of web.

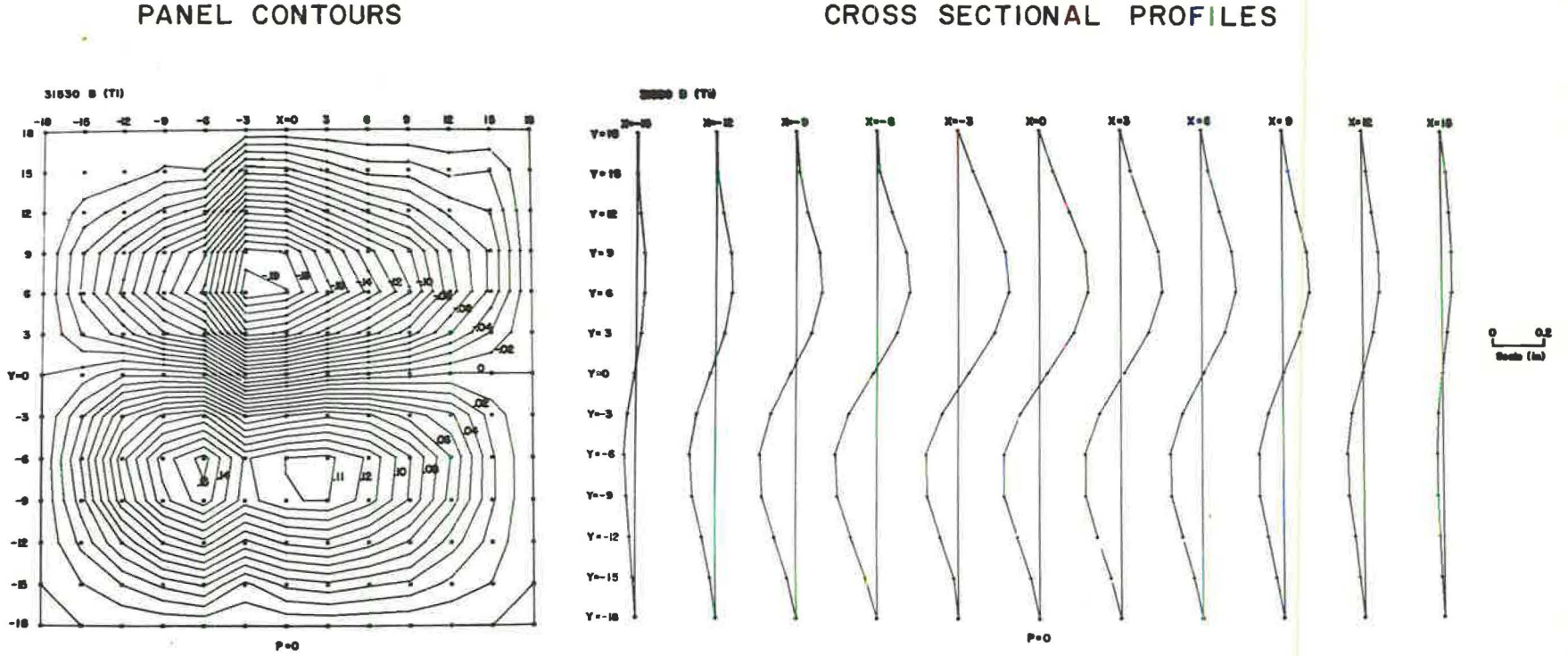

Figure 3. Double curvature initial deformation of web.

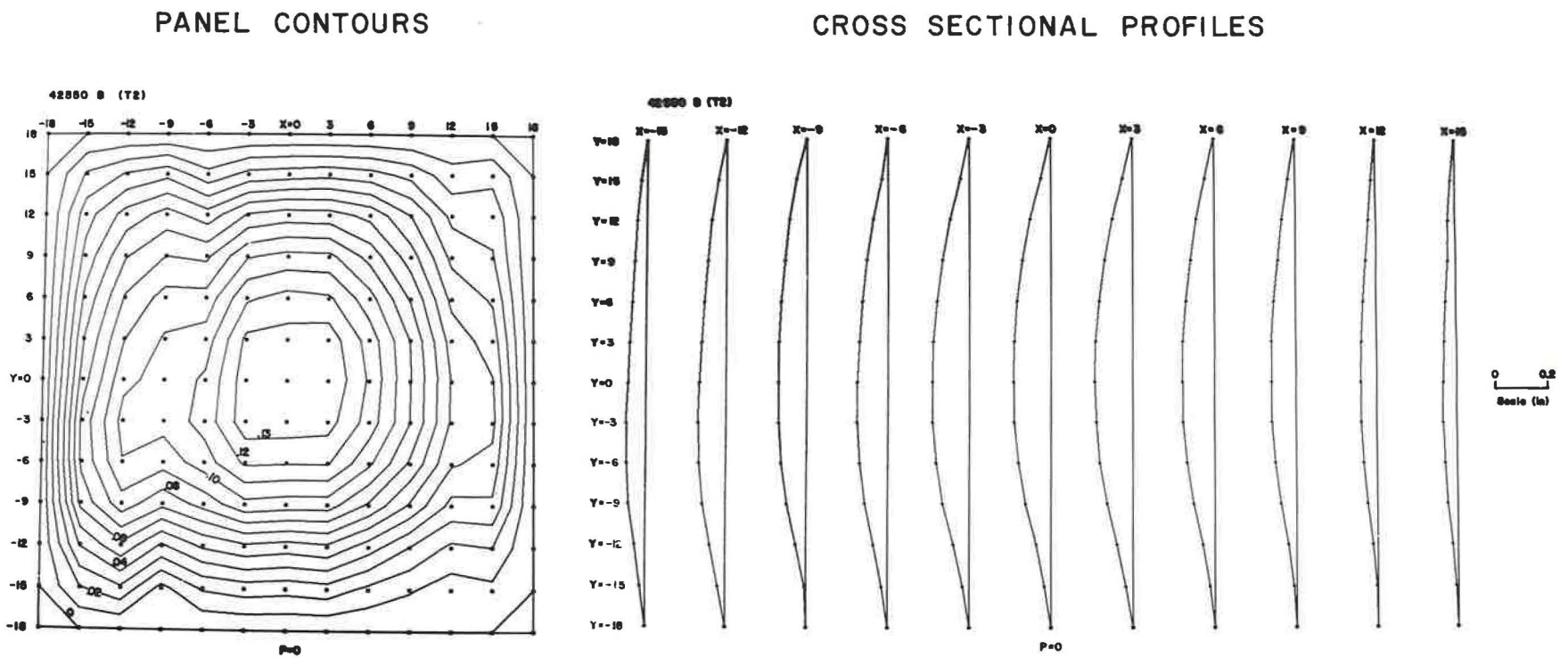

Figure 4. Single curvature initial deformation of web.

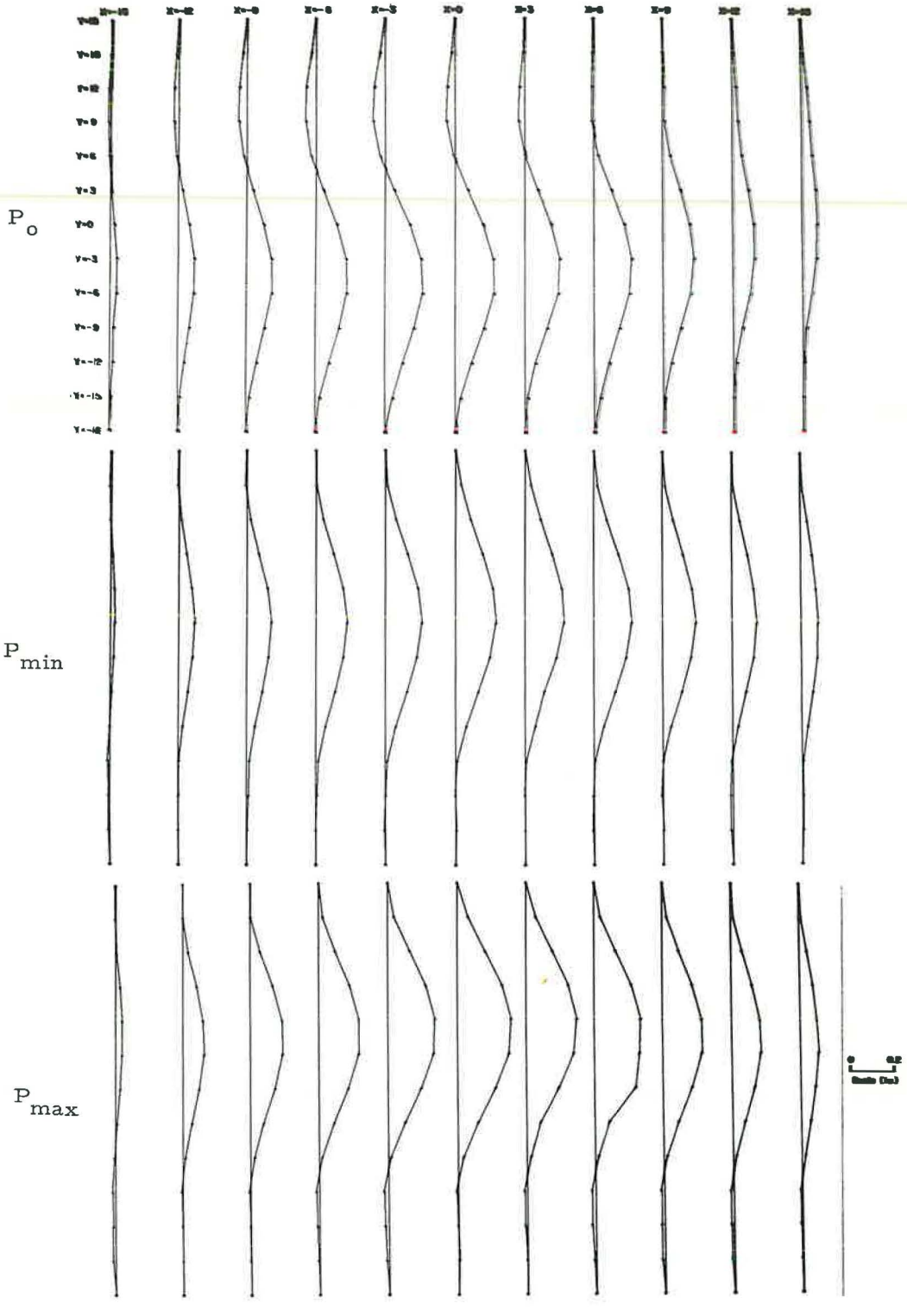

Figure 5. Change in shape of web cross section under increasing load (31020B).

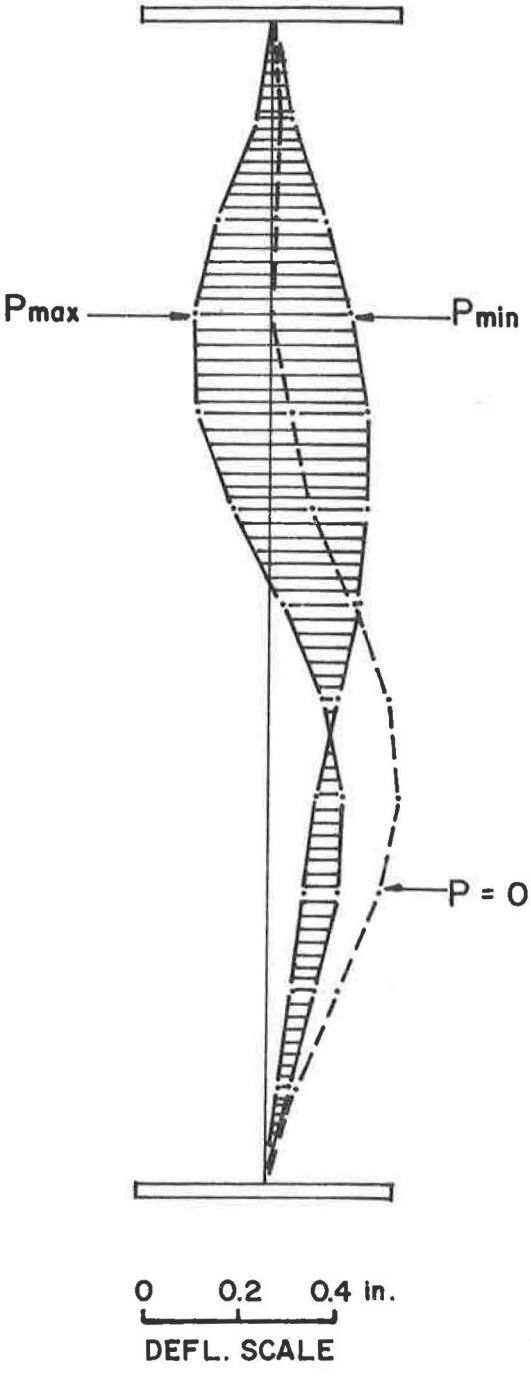

Figure 6. Movements of web under the applied load.

Because the Type 2 cracks were motivated by flexural stresses due to applied load, they propagated much faster than the Type 1 cracks. The cracks extended both upward and downward along the toe of the web-to-stiffener fillet weld. When this crack reached the tension flange, it propagated into it and led to a fracture, thereby causing the final failure of a girder. The sequential progress of such a crack is shown in Figure 10.

Type 3 Cracks

The Type 3 cracks are subdivided into 3 groups according to their origin (Fig. 7). The first group, Type 3a, includes those cracks which originated at the flange-to-web juncture. Such cracks were formed because of discontinuities on the fillet weld surface as a result of manual welding operations (Fig. 11).

The second group, Type 3b, includes those cracks which started at the edge of the tension flange. The cause of such a crack was the presence of notches at the edge of the plate as a result of the flame cutting process. Such notches may be formed by a sudden increase in oxygen pressure in the cutting torch or uneven travel of the cutting torch.

The third group, Type 3c, includes those cracks which originated at the reentrant corners of the tension flange. This type of crack was observed only in the panel specimens.

Repairs made on these cracks were found to be unsuccessful, and this was the main reason for changing from the panel specimens to the full-length specimens.

TEST RESULTS AND DISCUSSION

The number of cycles to initial crack formation for each test specimen is given in Table 2; also listed are web slenderness ratios based on actual measured dimensions and flange extreme fiber strains which correspond to the maximum and minimum stress levels. The ratio of strains larger than 1.0 implies that the web extreme fibers were strained beyond the elastic limit. The types of crack are also indicated.

To find a correlation between the fatigue strength and the thickness of web, an average number of cycles to initial crack

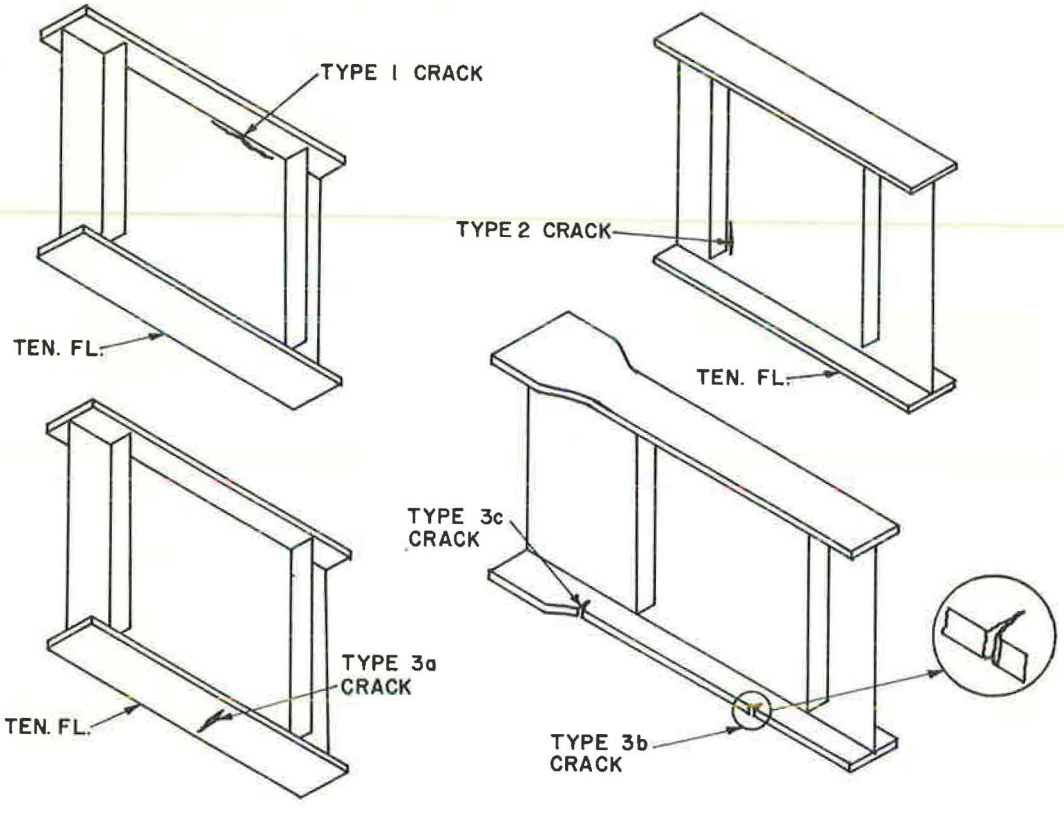

Figure 7. Types of fatigue crack.

is evaluated for each group of specimens having the same thickness. In computing the average values all runout test points were assumed as 2 million cycles, as this was the maximum expected fatigue life. Furthermore, since each group had a different number of specimens, weighed arithmetic means were computed to obtain unbiased average values. The average values so calculated and the dispersion of the data of each group are shown as a bar chart (Fig. 12). Each bar shows minimum, average and maximum number of cycles.

Figure 12 reveals that there is no strong interacting relationship between fatigue life and web thickness. Moreover, the wide range in fatigue life of each group shows that even if a certain relationship exists between the fatigue life and the web thickness, the regression analysis will indicate very poor correlation. Based on the test results as indicated by Figure 12, it can be said that the web thickness does not have a strong effect on the fatigue life of such girders.

To examine the influence of the applied stresses on the fatigue strength, irrespective of the web thickness, an average number of cycles to initial crack for each group of specimens which had the same stress range and minimum stress is calculated, assuming that all runouts lasted 2 million cycles. The average values are shown in Figure 13.

Test results appear to show that an increase in the stress range, that is, an increase in algebraic difference between the maximum and minimum stress, with a constant minimum stress, caused more significant reduction in fatigue life than an increase in the minimum stress with a constant stress range. For example, in Figure 13 the average value of the fatigue life for specimens subjected to 15-ksi stress range (15 to 30 ksi and 25 to 40 ksi) had more than twice the average fatigue life of those specimens subjected to 25-ksi stress range (15 to 40 ksi and 25 to 50 ksi). How-

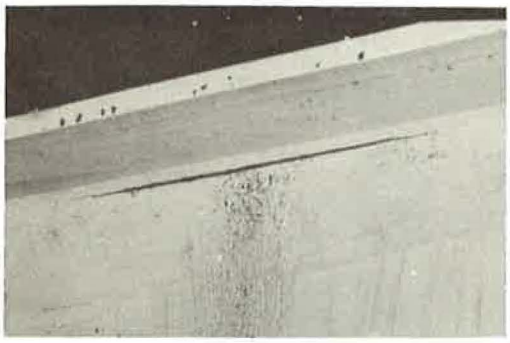

Figure 8. Crack in compression side of web along the toe of the web-to-flange fillet weld.

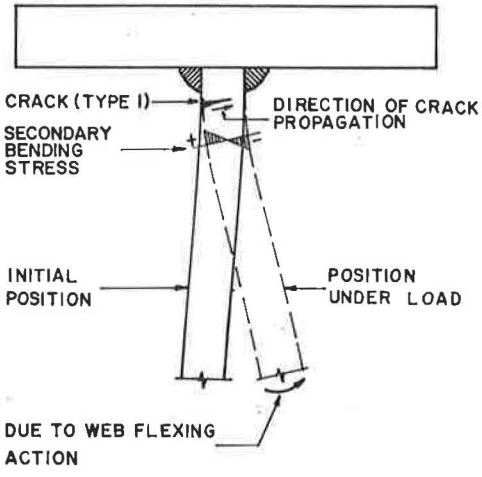

Figure 9. Development of Type 1 crack.

(1)

(2)

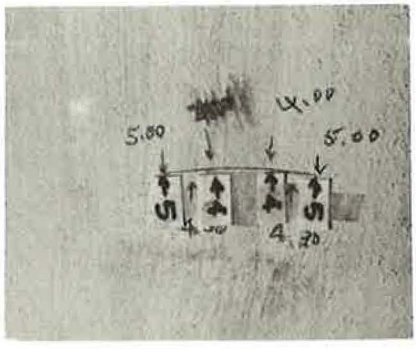

(3)

(4)

Figure 10. Sequential propagation of a Type 2 crack; (3) shows bottom face of tension flange.

TABLE 2

FATIGUE TEST RESULTS

Specimen	β	$\epsilon_{max}/\epsilon_{yw}$	$\epsilon_{min}/\epsilon_{yw}$	Cycles to Initial Crack	Type of Crack
21020A	295	0. 584	0. 292	2, 927, 000	No crack
21530A	295	0. 875	0. 437	2, 000, 000	No crack
21540A	295	1. 168	0. 437	294, 000	1
22540A	295	1. 168	0. 730	1, 318, 700	3c
				1, 722, 400	1
22550A	295	1. 470	0. 730	617, 800	1, 2
21020B	269	0. 603	0. 301	2, 233, 000	No crack
21530B	269	0. 905	0. 452	2, 137, 300	No crack
21540B	269	1. 206	0. 447	277, 400	Testing discontinued
22540B	269	1. 206	0. 749	1, 588, 000	1
22550B	269	1. 500	0. 749	672, 000	1
31020B	190	0. 476	0. 238	4, 770, 900	No crack
31530B	190	0. 714	0. 357	2, 104, 360	No crack
31540B	190	0. 953	0. 357	890, 000	2
				919, 000	2
				1, 132, 100	2
32540B	190	0. 953	0. 596	2, 440, 000	No crack
32550B	190	1. 192	0. 596	815, 300	1
				911, 530	3b
41020A	141	0. 525	0. 262	2, 311, 200	No crack
41530A	141	0. 798	0. 399	2, 000, 000	No crack
41540A	141	1. 060	0. 399	630, 000	3a
42540A	141	1. 060	0. 662	947, 200	3c
42550A	141	1. 325	0. 662	639, 500	3c
41530B	147	0. 702	0. 350	2, 052, 800	No crack
41540B	147	0. 935	0. 351	974, 000	2
				974, 000	2
42540B	147	0. 935	0. 604	3, 643, 000	No crack
42550B	147	1. 208	0. 604	421, 000	2
61530A	93	0. 700	0. 350	2, 000, 000	No crack
61540A	93	0. 935	0. 350	1, 394, 800	2,3a
62540A	93	0. 935	0. 548	2, 530, 000	No crack
62550A	93	1. 168	0. 584	479, 000	3b

Note: β based on measured dimension.

ϵ_{max}, ϵ_{min} = maximum and minimum yield strain of extreme fibers.

ϵ_{yw} = yield strain of web.

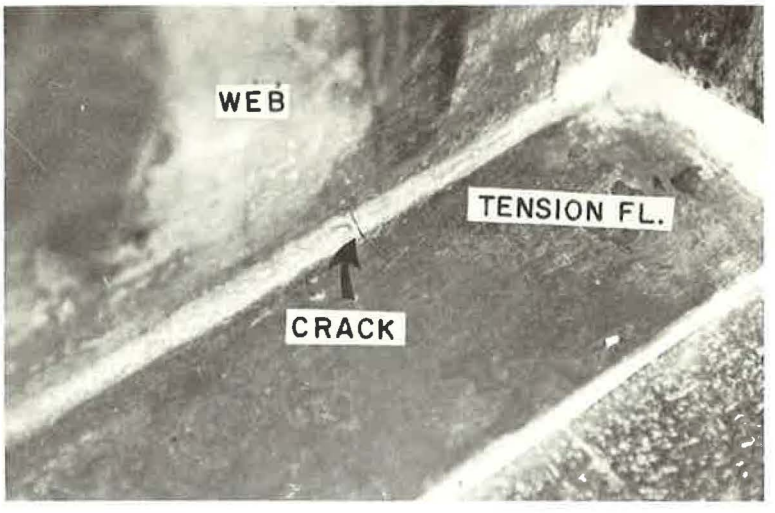

Figure 11. Crack initiating at discontinuity in the web-to-tension flange fillet weld.

ever, when a comparison is made between the specimens subjected to the same range of stresses of 15 ksi, but with different levels of minimum stress, as, for instance, from 15 to 30 ksi and from 25 to 40 ksi, no drastic drop in the average fatigue life was observed. A similar trend is also seen if the average fatigue life of the specimens subjected to the 15-ksi to 40-ksi range is compared with that of the specimens subjected to the 25-ksi to 50-ksi range.

It appears, therefore, that a change in the range of stress with a constant minimum stress has a greater influence on fatigue life than a change in the minimum stress with constant stress range.

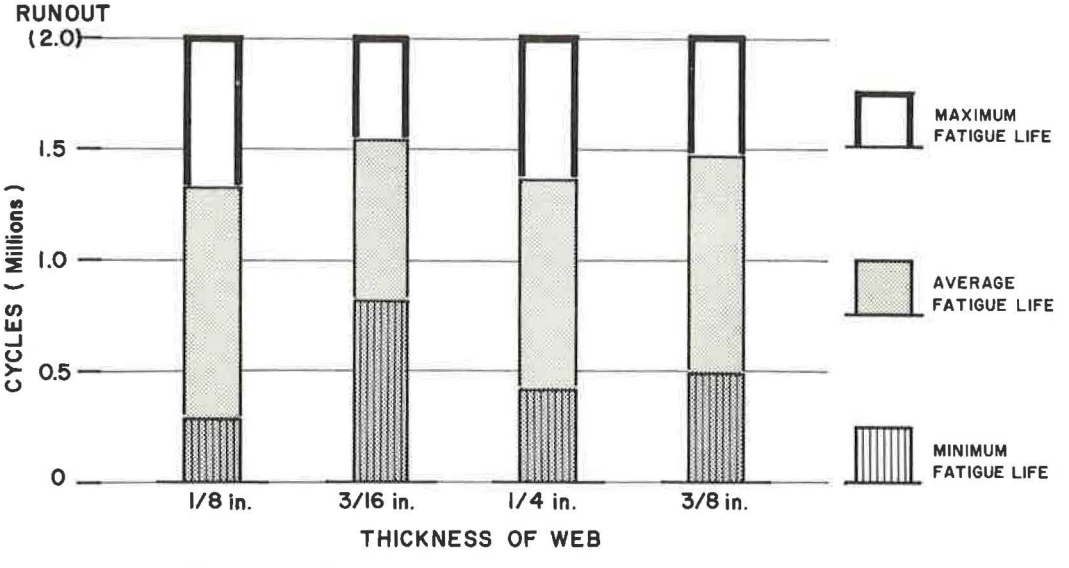

Figure 12. Average fatigue strength of specimens having the same web thickness.

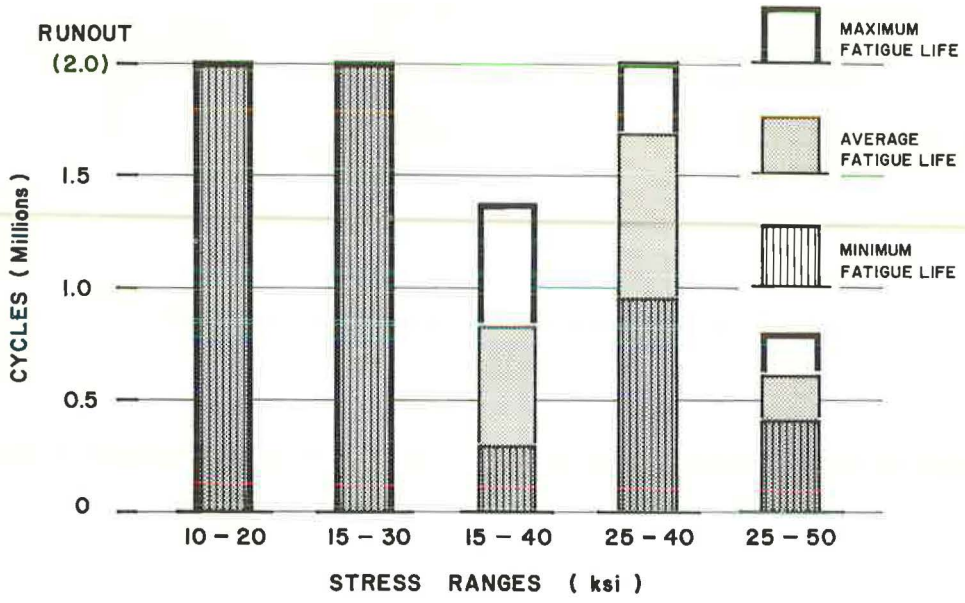

Figure 13. Average fatigue strength of specimens subjected to the same range of stress and minimum stress.

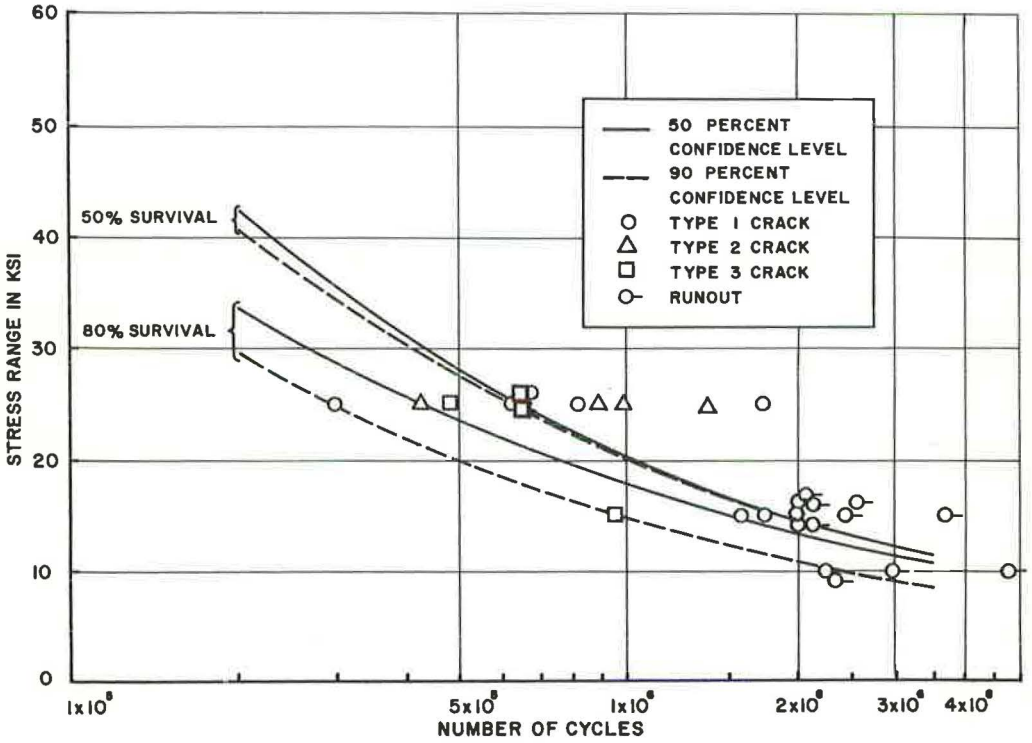

Figure 14. Probability-stress-cycle (P-S-N) curves.

ANALYSIS OF TEST RESULTS

No attempts were made to establish the shape of fatigue life distribution. Instead of speculating on a particular functional form which would satisfy the distribution of the data, probability-stress-cycle (P-S-N) curves are evaluated based on a technique suggested by ASTM (4) using the tabulated values of probability given by Schuette (5). This technique enables one to determine the P-S-N curve without knowledge of the shape of fatigue life distribution.

Fatigue life survival curves so determined are given in Figure 14; stress range is taken as the ordinate, since it was shown to be the most influencing factor on fatigue life. Probability survival curves of 50 and 80 percent corresponding to 50 and 90 percent confidence level are drawn to indicate the scatter of the test points. Actual test points are also plotted for reference.

A survival percentage of 50 corresponds to the median of a group. Since, in practice, values of percent survival less than 50 usually are not wanted, the 50 percent line can be considered as a limiting percentage survival line.

Confidence level values describe the accuracy of survival percentages. For example, a 50 percent survival corresponding to a 90 percent confidence level means that at least 50 percent of the population will survive N cycles (or fall above that line), and only 10 percent of such a statement are expected to be incorrect.

For comparison, in Figure 15 are plotted the test points of previous hybrid girder investigations (2) and two test points of homogeneous girder of A36 steel (6) against an 80 percent survival curve at 50 percent confidence level (80/50 curve). The hybrid girders were subjected to a stress range from 25 to 45 ksi. Except for one test point which had 141,000 cycles, the points agree reasonably well with the 80/50 curve.

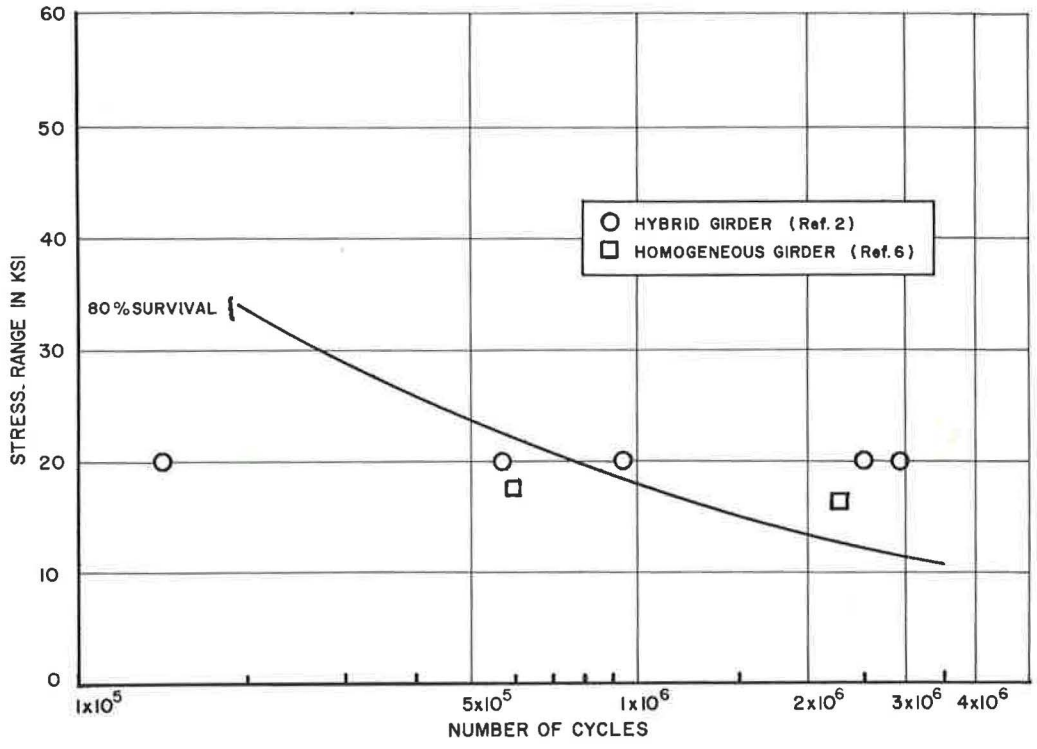

Figure 15. Test results of previous hybrid girders and homogeneous girders of A 36 steel.

The homogeneous girders were subjected to stress ranges of 17. 6 and 16. 6 ksi for the specimens which had initial crack at 600, 200 and 2, 280, 000 cycles, respectively. It should be mentioned that the one which survived to ?. 28 million cycles had previously been subjected to 13. 8-ksi stress range up to 1. 3 million cycles. Since one test point falls below and the other above the 80/50 line, no conclusion can be drawn as to how well the S-N curve of hybrid girders can estimate the fatigue life of the homogeneous girders. However, the comparison indicated that when estimates are based on the stress range, the fatigue life of hybrid girders and homogeneous girders are within a tolerable range.

CONCLUSIONS

The fatigue strength of hybrid plate girders made of ASTM A 514 steel flanges and A 36 steel web has been investigated. Statistical analyses were made on the test results and probability survival curves were evaluated. From this investigation, the following conclusions can be drawn:

1. The difference in web thickness did not show any significant change in fatigue strength.
2. Test results indicate that increasing the range of stress with a constant minimum stress level had a greater influence on fatigue life than raising the level of minimum stress with a constant stress range.
3. Based on the current test, fatigue life between 500, 000 and 2 million cycles can be estimated conservatively by the 80 percent survival curve at 50 percent confidence level (Fig. 14).

Further investigations are needed to establish a relationship between stress range and fatigue life in the lower range of cycles.

ACKNOWLEDGMENTS

This investigation is a part of the hybrid plate girder research program conducted at the Structures Fatigue Research Laboratory, The University of Texas, under the direction of Dr. A. A. Toprac. This research was sponsored by the Texas Highway Department, the U. S. Bureau of Public Roads and the American Iron and Steel Institute. The authors are indebted to A. L. Elliot, E. L. Erickson, W. Henneberger, T. R. Higgins, C. G. Schilling, and I. M. Viest (chairman) of the Texas Plate Girder Supervisory Committee.

Assistance during the test program was provided by research assistants at the Structures Fatigue Research Laboratory and, in particular, by D. Eyre and H. Toyoda. The authors are grateful for their help.

REFERENCES

1. Toprac, A. A., and Engler, R. A. Plate Girders With High Strength Steel Flanges and Carbon Steel Webs. Proc. National Engineering Conf., AISC, 1961.
2. Toprac, A. A. Fatigue Strength of Hybrid Plate Girders. SFRL Rept. No. 04-64, Univ. of Texas, 1964.
3. AASHO. Standard Specifications for Highway Bridges. Washington, D. C., 1961.
4. ASTM Committee E-9. A Guide for Fatigue Testing and the Statistical Analysis of Fatigue Data. STP No. 91-A, 1963.
5. Schuette, E. H. The Significance of Test Results From Small Groups of Specimen. Proc. ASTM, Vol. 57, 1957.
6. Yen, B. T., and Muller, J. A. Fatigue Tests of Large-Size Welded Plate Girders. Welding Research Council Bull. No. 118, Nov. 1966.

Lateral Distribution of Load in Composite Box Girder Bridges

S. B. JOHNSTON and A. H. MATTOCK, Respectively, Former Graduate Student and Professor of Civil Engineering, University of Washington

A computer program for the analysis of folded plate structures of general form was used to study the lateral distribution of load in simple span composite box girder bridges without transverse diaphragms or internal stiffeners. The results were used to develop simple expressions for the loads carried by the interior and exterior girders in this type of bridge.

The accuracy of the analysis was confirmed by the results of tests of a quarter-scale model of a two-lane, 80-ft span bridge supported by three box girders.

•THE type of bridge under consideration consists of trapezoidal section steel girders made composite with a reinforced concrete deck slab. A typical cross section is shown in Figure 1. Diaphragms are provided only at the supports and the girders are not stiffened internally in any way. Composite action is ensured by the provision of stud type shear connectors on the top flanges of the girders.

It is considered that bridges of the type described should be more efficient, economical and aesthetically pleasing than steel-concrete composite bridges using I-section girders. Due to the larger torsional stiffness of the closed trapezoidal section girder as compared to an I-section girder of similar flexural strength, a greater lateral distribution of loads is achieved with this form of construction than is the case with a concrete deck slab on steel I-section girders. The bending moment for which each girder must be designed is therefore less in the box girder bridge, thus leading to economy. Further economies in fabrication and erection are achieved by the elimination of stiffeners and transverse diaphragms other than at the supports. The clean external appearance of this type of bridge is aesthetically very pleasing.

METHOD OF ANALYSIS

A box girder bridge of the type described may be considered as a simply supported folded plate structure, since it consists of a series of adjoining thin plates rigidly connected along their edges, and since the end diaphragms effectively prevent displacements in their planes but offer negligible resistance normal to these planes.

A computer program was written for the analysis of simply supported folded plate structures of general form. The stiffness method of analysis was used allowing four degrees of freedom at each joint (1 rotational, 3 translational). The stiffness coefficients used were obtained from the exact solution of the folded plate problem produced by Goldberg and Leve (1). The computer program is discussed in more detail elsewhere (2).

For a given load system the computer program yields the displacements and forces acting at each joint. To obtain displacements and stresses within a plate, the plate is hypothetically subdivided into a number of coplanar plates joined at their edges. The displacements and stresses at the locations of the hypothetical joints can then be obtained by use of the computer program.

Paper sponsored by Committee on Steel Superstructures and presented at the 46th Annual Meeting.

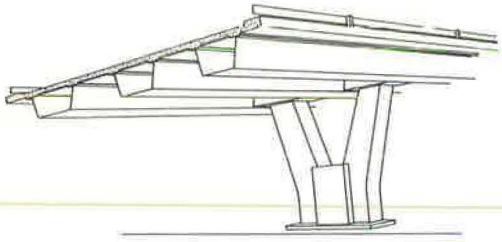

Figure 1. Typical composite box girder bridge.

RELIABILITY OF THE ANALYSIS

The folded plate theory assumes that the materials of which the structure is made are linearly elastic and that the constituent plates are isotropic in their properties. An actual bridge structure is unlikely to satisfy these assumptions exactly, although it should come close to doing so at service load level. Of particular relevance is the behavior of the reinforced concrete deck slab which is neither isotropic nor perfectly elastic. To provide a check on the analysis and computer program, it was decided to build and test a one-quarter scale model of an 80-ft span, two-lane highway bridge of the type under consideration. A detailed description of the fabrication and testing of this model is given elsewhere (2, 3).

Design of Test Bridge

Particulars of the design of the prototype bridge are as follows:

Span—80 ft
Number of lanes—2
Width of roadway—28 ft
Overall width of bridge—34 ft
Number of box girders—3
Design Load—HS20-44
Assumed AASHO Load Distribution Factor—S/6. 5
Steel in box girders—type ASTM A 36 (allowable stress 20 ksi)
Deck slab reinforcement—Intermediate grade
Deck slab concrete strength $-f'_c$ = 4000 psi

The use of an AASHO load distribution factor of S/6. 5 was based on judgment. It was anticipated that the lateral load distribution characteristics of this type of bridge

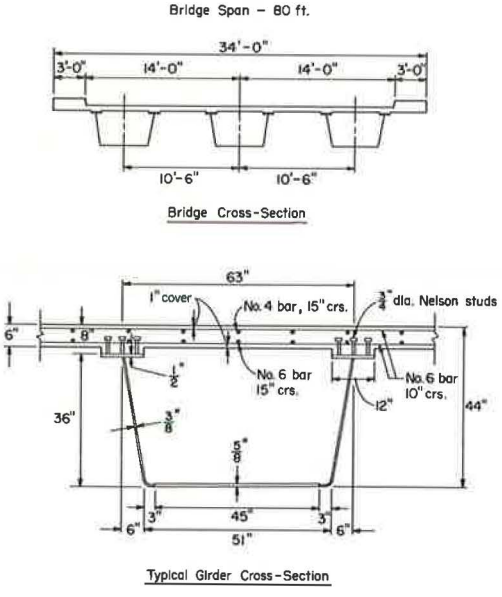

Figure 2. Dimensions of prototype bridge.

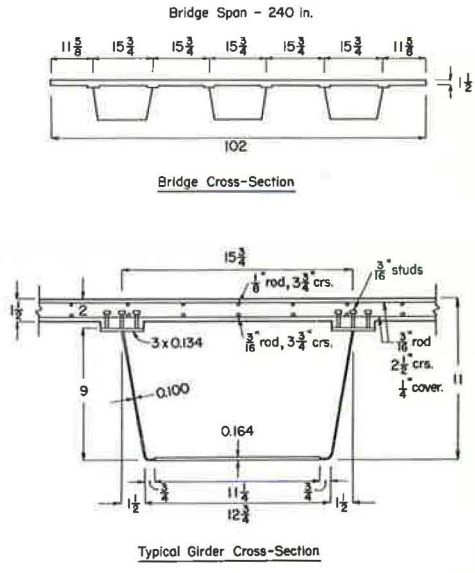

Figure 3. Dimensions of model bridge (inches).

TABLE 1

TRUE SCALE AND ACTUAL PLATE THICKNESSES

Dimension	Prototype (in.)	True Scale (in.)	Actually Used (in.)
Top flange thickness	0. 500	0. 125	0. 134
Web thickness	0. 375	0. 096	0. 100
Bottom plate thickness	0. 625	0. 156	0. 164

would be somewhat better than those of composite bridges with I-section girders for which the AASHO load distribution factor is S/5. 5. The tests and analytical studies subsequently made showed that this was a reasonable assumption.

The design for flexure was in accordance with Section 9 of the 1961 AASHO specifications (4). It was assumed that the trapezoidal section steel girder would act alone when carrying its own weight and that of the concrete slab, and that the composite section would resist the live load moments and those due to the weight of the curbs, guardrails, etc.

The design for shear was in accordance with paragraph 1. 6. 409 of the 1963 AASHO Interim Specifications (5). The webs were made the minimum thickness permitted without the use of stiffeners.

The concrete deck slab was made the thinnest possible to resist the design bending moments specified in AASHO specifications. Since the lateral distribution of loads is very dependent on the stiffness of the deck slab, use of the thinnest possible slab will yield the worst lateral distribution for a given girder size and configuration.

The cross section of the prototype bridge is shown in Figure 2. As far as possible the model was made a true quarter-scale model of the prototype bridge. The only deviations were in the thicknesses of the steel plate used in the fabrication of the trapezoidal girders. The deviations arose because of the necessity of using available standard thicknesses of steel sheet metal. They are as shown in Table 1.

The dimensions of the test model are shown in Figure 3. The actual dimensions of the model were used when calculating its behavior using the computer program.

The deck slab was of reinforced mortar to simulate the reinforced concrete of the prototype. The bar sizes and spacing were reproduced exactly to scale. At the time of test the mortar had a compressive strength of 3340 psi, somewhat less than the 4000-psi concrete strength assumed in the prototype design.

Comparison of Calculated and Actual Behavior

Two types of test were carried out on the model bridge, influence line tests and truck loading tests.

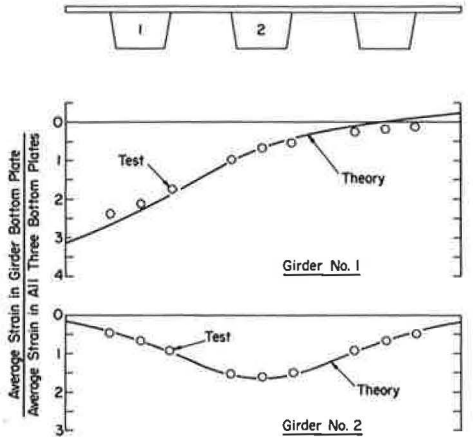

Figure 4. Influence lines for average strain in bottom plate of girders 1 and 2 of the model bridge.

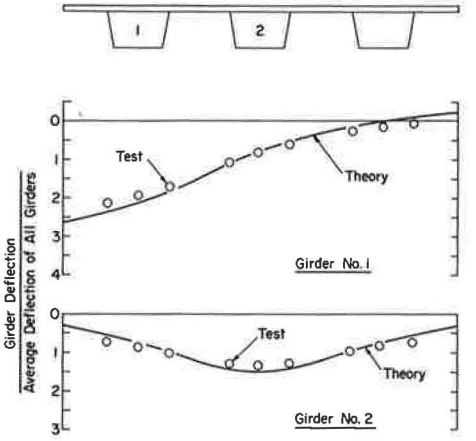

Figure 5. Influence lines for girder deflection in model bridge.

Influence Line Tests—In these tests a concentrated load was placed at nine successive locations across the width of the bridge at midspan. For each location of the load, the deflections of the girders and the strains in the bottom plates of the girders were measured. It was thus possible to construct experimentally transverse influence lines for deflection of each girder and for average strain in the bottom of each girder. This last may be regarded as a measure of the bending moment carried by each girder.

The experimental influence line ordinates are plotted in Figures 4 and 5 together with the influence lines calculated using the folded plate computer program. The agreement is seen to be good, the actual behavior of the model being slightly better than the calculated behavior. The calculated influence lines are based on the first three terms of the Fourier series representing a concentrated load.

Truck Loading Tests—In these tests six concentrated loads were applied to the bridge deck simultaneously. The distribution and relative magnitudes of these loads simulated to one-quarter scale the wheel loads of the HS20-44 AASHO standard design truck load. The loads were applied by placing a block of concrete on top of an articulated steel frame resting on the bridge deck as shown in Figure 6. Measurements were made at midspan of girder deflection and strain in the girder bottom plates.

The loads were applied in both lanes of the bridge, in the extreme lateral positions as considered in design that the truck can occupy. In Figure 7a the measured deflections are compared with the calculated deflections for the truck loading placed as close to the curb as is required by AASHO specifications. Similarly, in Figure 7b the deflections are plotted for the case of the truck loading placed as close to the center line of the bridge as required by AASHO specifications. The agreement between measured and calculated behavior is seen to be close in both cases, with the bridge once again behaving a little better than was calculated.

By superposing the results obtained in these tests it was possible to obtain the distribution of wheel loads between the three supporting box girders when two standard trucks are placed on the bridge, (a) so as to produce maximum moment in an exterior girder, and (b) so as to produce maximum moment in the interior girder. The experimentally determined distributions of load are compared in Figure 8 with the distributions of load obtained from the calculated deflection influence lines, it being assumed that the total load is distributed between the three girders in proportion to their midspan deflections. It can be seen that the calculated transverse distribution of loads is in close agreement with the measured distribution, and in particular that the calculated maximum loads carried both by an exterior girder and by an interior girder are in very close agreement with the measured maximum loads.

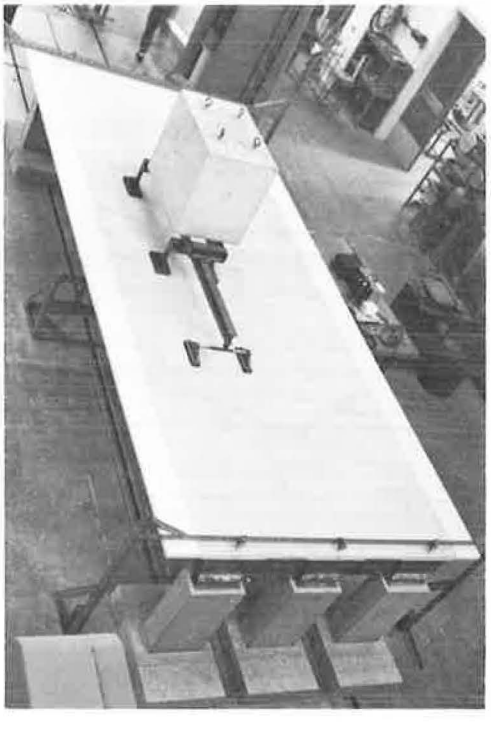

Figure 6. Truck loading test of model bridge.

The measured maximum loads carried by an exterior girder and by the interior girder are respectively equivalent to AASHO load distribution factors of S/6. 91 and S/6. 48. This result justifies the prior assumption of a load distribution factor of S/6. 5 in the design of the prototype bridge.

The close agreement between the observed behavior of the model bridge and the behavior predicted by the folded plate theory computer program indicates that the program is reliable and can reasonably be used to predict the behavior of other bridges of this type.

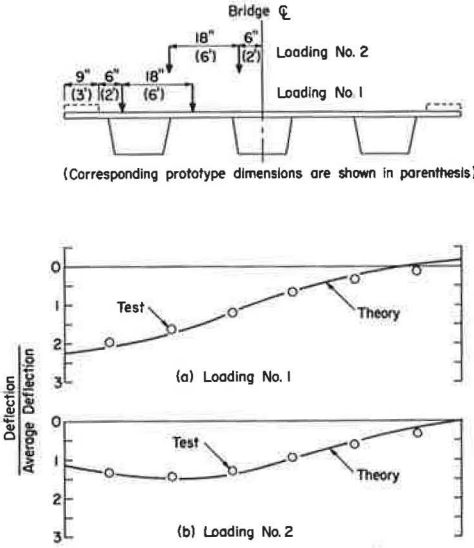

Figure 7. Midspan deflections of model bridge in truck loading tests.

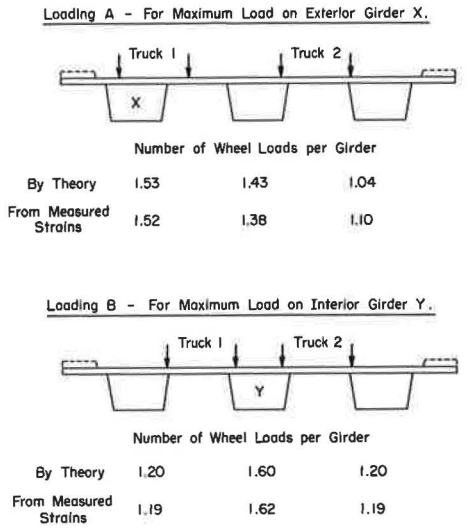

Figure 8. Comparison of theoretical and actual distribution of loads—truck loads placed to produce maximum loads in particular girders.

ANALYTICAL STUDY

The folded plate theory computer program was used to calculate the behavior of a series of 24 composite box girder bridges, covering a fairly wide range of spans, numbers of lanes, and numbers of girders. The spans included were 50, 75, 100 and 150 ft. For each span the following combinations of numbers of lanes and numbers of box girders were considered: (a) 2 lanes, 2 or 3 box girders; (b) 3 lanes, 3 or 4 box girders; and (c) 4 lanes, 4 or 5 box girders.

The lane widths used for the 2-, 3- and 4- lane bridges were 14 ft 0 in., 12 ft 0 in. and 12 ft 3 in. respectively. A curb width of 3 ft was used in all cases.

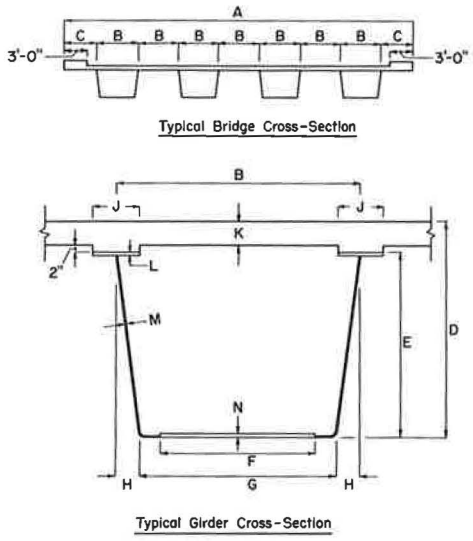

Figure 9. Typical midspan cross sections for bridges considered in analytical study.

The particulars of the design of these bridges are the same as for the design of the prototype bridge on which the test model was based. The dimensions of the midspan cross section of each bridge are given in Table 2 (dimension letters refer to Fig. 9). In each case the thickness of the deck slab was arrived at by consideration of its action as a slab spanning transversely across the top flanges of the trapezoidal section girders. The minimum possible thickness of slab was used in each case so that the calculated values of lateral distribution of load should be conservative.

For each girder of each of the bridges, influence lines were calculated showing the load carried by the girder under consideration as a unit load moves transversely across the bridge at midspan. These influence lines were based on the calculated behavior of the bridges, assuming that the load is divided between the girders in proportion to their center-line deflections.

TABLE 2

DIMENSION SUMMARY FOR BRIDGES CONSIDERED IN ANALYTICAL STUDY

Bridge No.	Span (ft)	No. of Lanes	No. of Girders	Dimension (See Fig. 9)[a]												
				A	B	C	D	E	F	G	H	J	K	L	M	N
50-1	50	2	2	34 ft 0 in.	96	60	29	20	76	88	4	12	7	5/8	3/8	1/2
50-2	50	2	3	34 ft 0 in.	63	46 1/2	28	20	43	55	4	12	6	1/2	3/8	1/2
50-3	50	3	3	44 ft 6 in.	86	52	28 3/4	20	60	78	4	12	6 3/4	9/16	3/8	1/2
50-4	50	3	4	44 ft 6 in.	63	46 1/2	28	20	43	55	4	12	6	1/2	3/8	1/2
50-5	50	4	4	55 ft 0 in.	80	50	28 1/2	20	60	72	4	12	6 1/2	1/2	3/8	1/2
50-6	50	4	5	55 ft 0 in.	63	46 1/2	28	20	43	55	4	12	6	1/2	3/8	1/2
75-1	75	2	2	34 ft 0 in.	96	60	44	35	72	84	6	13	7	3/4	7/16	5/8
75-2	75	2	3	34 ft 0 in.	63	46 1/2	43	35	39	51	6	12	6	5/8	3/8	5/8
75-3	75	3	3	44 ft 6 in.	86	52	43 3/4	35	62	74	6	13	6 3/4	3/4	3/8	5/8
75-4	75	3	4	44 ft 6 in.	63	46 1/2	43	35	39	51	6	12	6	5/8	3/8	5/8
75-5	75	4	4	55 ft 0 in.	80	50	43 1/2	35	56	68	6	12	6 1/3	3/4	3/8	5/8
75-6	75	4	5	55 ft 0 in.	63	46 1/2	43	35	39	51	6	12	6	5/8	3/8	5/8
100-1	100	2	2	34 ft 0 in.	96	60	58	49	72	84	6	14	7	1	1/2	3/4
100-2	100	2	3	34 ft 0 in.	63	46 1/2	57	49	39	51	6	12	6	3/4	7/16	3/4
100-3	100	3	3	44 ft 6 in.	86	52	57 3/4	49	62	74	6	13	6 3/4	1	7/16	3/4
100-4	100	3	4	44 ft 6 in.	63	46 1/2	57	49	39	51	6	12	6	3/4	7/16	3/4
100-5	100	4	4	55 ft 0 in.	80	50	57 1/2	49	56	68	6	12	6 1/3	1	7/16	3/4
100-6	100	4	5	55 ft 0 in.	63	46 1/2	57	49	39	51	6	12	6	3/4	7/16	3/4
150-1	150	2	2	34 ft 0 in.	96	60	85	76	72	84	6	14	7	1 1/2	5/8	1
150-2	150	2	3	34 ft 0 in.	63	46 1/2	84	76	41	51	6	13	6	1	1/2	1
150-3	150	3	3	44 ft 6 in.	86	52	84 3/4	76	58	70	8	13	6 3/4	1 1/2	9/16	1
150-4	150	3	4	44 ft 6 in.	63	46 1/2	84	76	41	51	6	13	6	1	1/2	1
150-5	150	4	4	55 ft 0 in.	80	50	84 1/2	76	52	64	8	12	6 1/2	1 1/2	9/16	1
150-6	150	4	5	55 ft 0 in.	63	46 1/2	84	76	41	51	6	13	6	1	1/2	1

[a]Dimensions are given in inches except for A, the overall width of the bridge.

It is thought that this procedure is justified by the agreement between the measured distribution of loads in the model bridge and the distribution of loads calculated using this assumption (Fig. 8). A typical set of influence lines is shown in Figure 10.

The maximum load carried by each girder of each bridge was calculated using the influence lines, the worst possible combinations of truck locations on the bridge deck being considered in each case. The maximum loads carried by each girder were expressed in terms of multiples of one "wheel load" of the AASHO standard truck and are summarized in Table 3, along with the values of N (in S/N, the AASHO load distribution factor) which correspond to the number of wheel loads carried by the girder and the center-to-center spacing of the box girders. No reduction in intensity of loads for simultaneous loading of more than two lanes was included in the calculation of the values shown in Table 3.

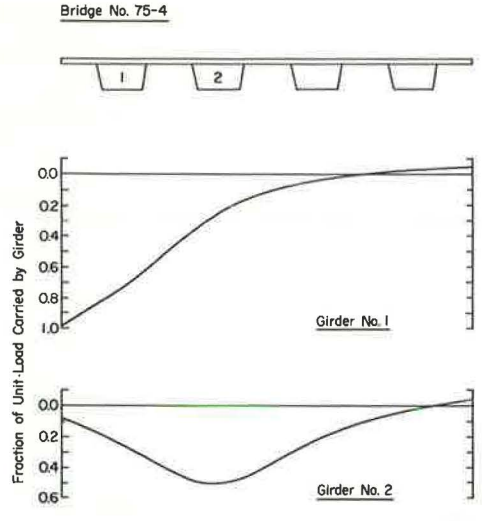

Figure 10. Typical girder load influence lines.

It can be seen in Table 3 that the values of N vary considerably both with span and type of bridge. An attempt was first made to correlate the values of N with span and some parameter related to the type of bridge, but this was not successful. The general trend of variation of N with span can readily be seen in Figure 11, where the average values of N are plotted for all except the two girder bridges. The

TABLE 3

SUMMARY OF CALCULATED MAXIMUM LOADS AND CORRESPONDING VALUES OF N

Bridge Type	Girder Spacing[a] (ft)	Girder No.[b]	Bridge Span (ft)							
			50		75		100		150	
			Wheel Loads[c]	N[d]	Wheel Loads[c]	N[d]	Wheel Loads[c]	N[d]	Wheel Loads[c]	N[d]
2-Lane, 2-Girder	16.00	1	2.18	7.35	2.16	7.41	2.12	7.56	2.11	7.59
2-Lane, 3-Girder	10.50	1	1.56	6.73	1.57	6.70	1.57	6.70	1.55	6.77
		2	1.70	6.18	1.63	6.44	1.58	6.65	1.51	6.95
3-Lane, 3-Girder	14.33	1	2.08	6.88	2.10	6.82	2.12	6.76	2.14	6.70
		2	2.42	5.93	2.35	6.10	2.30	6.23	2.18	6.57
3-Lane, 4-Girder	10.50	1	1.66	6.35	1.64	6.40	1.61	6.52	1.62	6.48
		2	1.88	5.58	1.81	5.80	1.72	6.12	1.67	6.28
4-Lane, 4-Girder	13.33	1	1.97	6.78	2.03	6.58	2.04	6.55	2.12	6.30
		2	2.32	5.75	2.34	5.70	2.26	5.90	2.30	5.80
4-Lane, 5-Girder	10.50	1	1.65	6.36	1.65	6.36	1.67	6.30	1.68	6.25
		2	1.88	5.58	1.80	5.83	1.77	5.93	1.75	6.00
		3	1.90	5.52	1.89	5.55	1.84	5.71	1.80	5.80

[a] Center-to-center spacing of box girders.
[b] Girders are numbered from outside to inside, i.e., girder No. 1 is an exterior girder.
[c] Maximum number of wheel loads carried by the particular girder.
[d] N in S/N, the AASHO load distribution factor.

average value of N for the exterior girders of all bridges except the two-lane, two-girder bridges was approximately a constant 6.6, with a range of variation of about ±0.25. The average value of N for the interior girders increases approximately linearly from 5.8 at 50-ft span to 6.3 at 150-ft span, with a range of variation of about ±0.45 for any particular span. The average value of N for the two-lane, two-girder bridge is about 7.5. With this variation in N, the difficulty of selecting a truly representative value of N for use in design is apparent. However, it should be noted that in all cases the average values of N were in excess of the value of 5.5 specified for the design of a composite bridge with I-section girders.

The coefficient N is only used in design in combination with the girder spacing to obtain the multiple of one wheel load for which each girder must be designed. In other words, N is a means to an end and not an end in itself. An attempt was therefore made to relate directly the maximum load carried by each girder and some simple characteristics of the bridges. It was found that the maximum number of wheel loads carried by an interior girder could be expressed in terms of two simple parameters:

$$S = \text{Bridge span in feet}$$

and

$$R = \frac{\text{Number of traffic lanes}}{\text{Number of box girders}}$$

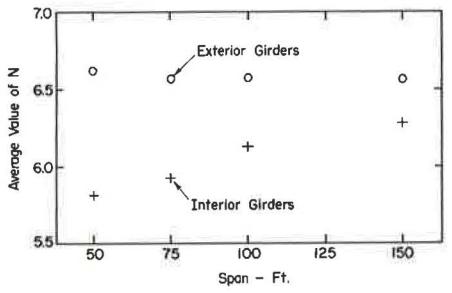

Figure 11. Variation of average value of N with span.

In Figure 12 the maximum number of wheel loads, W_i, carried by an interior girder in each bridge studied is plotted against the ratio R. It can be seen that the calculated values for all the bridges studied fall very close to the family of lines represented by

$$W_i = 0.42 + 2.08\,R - 0.002\,S \qquad (1)$$

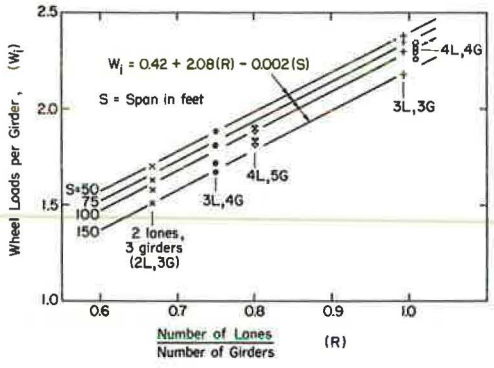

Figure 12. Maximum load carried by an interior girder.

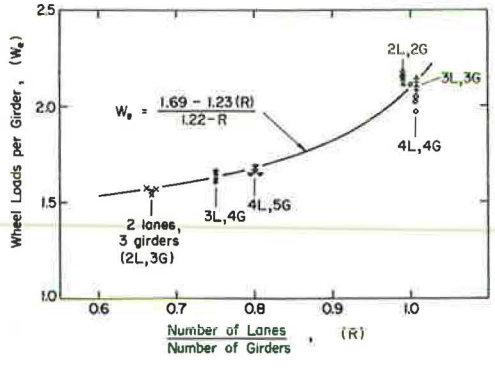

Figure 13. Maximum load carried by an exterior girder.

where W_i is the maximum number of wheel loads carried by one interior box girder, and R and S are as defined above.

Similarly, in Figure 13 the maximum number of wheel loads, W_e, carried by an exterior girder in each bridge studied is plotted against the ratio R. Since for a given value of R the maximum number of wheel loads carried by an exterior girder does not vary significantly with span, it is possible to express W_e in terms of R only, i.e.,

$$W_e = \frac{1.69 - 1.23\,R}{1.22 - R} \qquad (2)$$

where W_e is the maximum number of wheel loads carried by an exterior box girder and the ratio R is as before.

It is interesting to note that the behavior of the two-lane, two-girder bridges appears consistent with the behavior of the other bridges when the distribution of load is considered in this form, contrary to the situation when a correlation with the distribution factor N was attempted. Equation 2 predicts quite closely the behavior of all the bridges considered in this study.

Reduction in Load Intensity for Multiple Lane Loading

It was noted earlier that the maximum loads per girder were calculated without any reduction being made for simultaneous loading of more than two lanes. In each case the bridge was loaded so as to produce the worst condition for the girder under consideration; i.e., all lanes were not necessarily loaded in all cases.

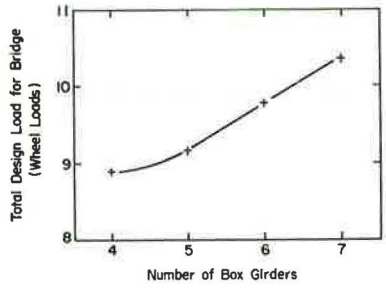

Figure 14. Variation of total design load with number of girders—4-lane bridge, 75-ft span.

When applying the provisions of Section 1.2.9, "Reduction in Load Intensity," of the AASHO specifications (4) to the loads given by Eqs. 1 and 2, it would be unconservative to base the reduction factor on the total number of traffic lanes on the bridge. On the basis of experience in analyzing the behavior of the bridges included in this study, it is proposed that the load intensity reduction factors used in conjunction with maximum loads calculated using Eqs. 1 and 2 should be based on one less than the total number of traffic lanes carried by the bridge.

Optimum Number of Girders

Using the equations proposed, the total number of wheel loads for which a bridge must be designed was calculated for a number of bridges with various combinations of numbers of lanes of traffic, numbers of box girders and lengths of span. For a bridge carrying a given number of lanes of traffic over a given span, in every case the total number of wheel loads for which the bridge must be designed was a minimum when one box girder was provided for each lane of traffic.

An example of the variation of total load-carrying capacity required with increasing number of box girders is shown in Figure 14. It appears therefore that the most economical arrangement of girders for this type of bridge is one box girder for each lane of traffic.

CONCLUSIONS

Agreement between the observed and calculated behavior of a one-quarter scale model of an 80-ft span composite steel-concrete box girder bridge without transverse diaphragms or internal stiffeners confirmed the applicability of folded plate theory to bridges of this type.

A study was made of the behavior of 24 composite box girder bridges using a computer program based on folded plate theory. As a result of the study, Eqs. 1 and 2 are proposed for the maximum number of wheel loads carried by the box girders in this type of bridge. Load intensity factors used in conjunction with maximum loads calculated using the given equations should be based on one less than the total number of traffic lanes carried by the bridge.

The study also indicated that the most economical arrangement of girders in this type of bridge was one box girder for each line of traffic.

ACKNOWLEDGMENTS

This investigation was carried out in the Structural Research Laboratory of the Department of Civil Engineering, University of Washington. Contributions were made by several members of the laboratory staff, to whom thanks is given.

The study was sponsored by the United States Steel Corporation.

REFERENCES

1. Goldberg, J. E., and Leve, H. L. Theory of Prismatic Folded Plate Structures. Internat. Assoc. for Bridge and Structural Eng., Publications, Vol. 16, 1957, pp. 59-86.
2. Johnston, S. B., and Mattock, A. H. An Experimental and Analytical Study of the Lateral Distribution of Load in Composite Box Girder Bridges. Final Report to United States Steel Corp., 1967.
3. Johnston, S. B., and Mattock, A. H. An Analytical and Model Study of Composite Box Girder Bridges. To be presented at ASCE Structural Conf., Seattle, May 1967.
4. American Association of State Highway Officials. Standard Specifications for Highway Bridges. Eighth Edition, 1961.
5. American Association of State Highway Officials. Interim Specifications, 1963. Developed by AASHO Committee on Bridges and Structures.

Prefabricated Composite Highway Bridge Units With Inverted Steel T-Beams

J. F. McDERMOTT, Senior Research Engineer, U. S. Steel Corporation, Applied Research Laboratory, Monroeville, Pa.

•TO MEET the current need of highway engineers for a low-cost prefabricated short-span bridge unit that can be rapidly erected, the U. S. Steel Applied Research Laboratory and the Indiana Steel Fabricators Association evolved a prefabricated bridge unit (Fig. 1) consisting of a concrete deck connected to two steel inverted T-beams by studs. It is intended that these units, including transverse bracing between the T-beams and including the deck, be prefabricated in steel fabricators' shops, transported to the bridge site by truck, placed side by side on the substructure, and field-connected by installing transverse tie rods through the deck and forcing nonshrinking grout into the longitudinal keyways between units. At this stage of construction, truck traffic could pass over the bridge. However, a bituminous wearing surface would probably be placed and railings installed before the bridge would be opened to traffic.

A main feature of these prefabricated composite bridges is that, unlike conventional composite beam bridges, the steel beams in these units have no top flanges. Although the top flange contributes little to the strength of a composite beam after the concrete deck has hardened, in conventional cast-in-place construction it does serve the important function of helping to support the dead weight of the concrete without excessive shoring or temporary supports. However, by prefabricating the units, the need for shoring is eliminated and the economy of steel T-beams can be fully realized. Another advantage of prefabrication is that most of the concrete shrinkage occurs before erection, and pre-erection shrinkage cracks parallel to the longitudinal axis of each unit would be unlikely. Thus, prefabrication greatly reduces the possibility of shrinkage cracks parallel to the longitudinal axis of the bridge in the finished structure.

This paper presents designs for units with inverted steel T-beams having several different unit widths (Fig. 2) and different spans. Although these designs are intended for prefabricated construction, they could also be used for cast-in-place construction if adequate shoring were employed. For cast-in-place construction, however, it would be more efficient to use an equal spacing of T-beams rather than the unequal spacing used in the prefabricated units.

GENERAL DESIGN REQUIREMENTS

The American Association of State Highway Officials (AASHO) Standard Specifications for Highway Bridges, eighth edition, 1961, was used as the design specification for this study, except for certain special live-load distribution formulas developed herein. HS20 live load was used in all beam designs, and a 16,000-lb wheel load (plus 30 percent for impact) was assumed in all deck designs. The weight of the bituminous wearing surface was assumed to be 30 psf.

All main material of the T-beams consists of high-strength structural steel conforming to ASTM designations A441 or A242. These steels, which have a yield strength of 50,000 psi for thicknesses up to $\frac{3}{4}$ in., inclusive, were chosen because of their superior strength-to-cost ratio; steels with higher yield strengths were not considered because of live-load deflection limitations. Greater economy could be achieved by the use of other commercially available high-strength low-alloy steels currently being considered for adoption by ASTM.

Paper sponsored by Committee on Steel Superstructures.

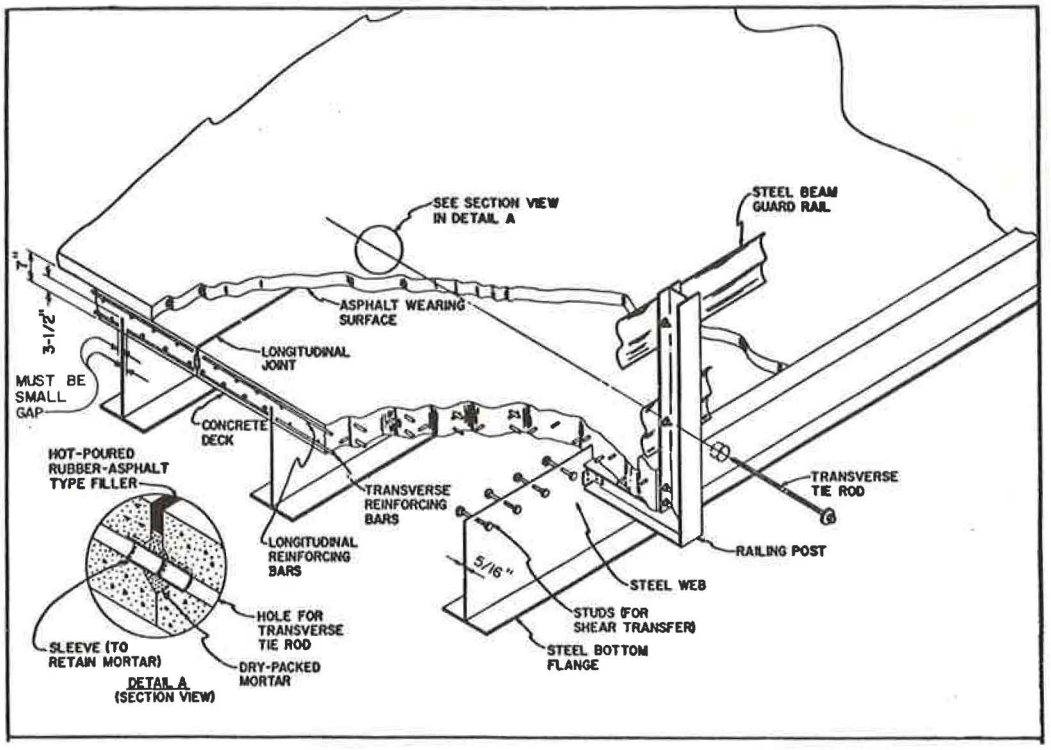

Figure 1. Prefabricated composite highway bridge unit with inverted steel T-beams.

Diaphragms, web stiffeners, railings, railing posts, and other detail material are made from A36 steel. Because the AASHO specification limits the minimum thicknesses of plates to $\frac{5}{16}$ in., all web plates were designed to be $\frac{5}{16}$ in. thick.

DESIGN OF DECK SLAB AS TRANSVERSE SPAN

The reinforced-concrete decks simultaneously perform two functions: (a) they act as transverse spans, distributing the wheel-load concentrations to the vertical web plates, and (b) they act as the top flanges of the longitudinal bridge beams. The first function, which governs reinforcing requirements and which generally governs the slab thickness, is discussed in this section; the second function is discussed in the following section.

For all designs, the concrete slabs are 7 in. thick because that appeared to be the minimum thickness practical to accommodate embedment of the beam webs and stud connectors, as well as positioning the holes for the transverse tie rods and placing the reinforcing steel. Concrete with 3,500-psi ultimate compression strength, which is within the 3,000-to-4,000 psi range most typical of bridge construction, was selected for all designs because many of the optimum beam designs, discussed next, result in longitudinal compression stresses in the deck close to the 1,400-psi allowable stress corresponding to 3,500-psi ultimate compression strength.

It was assumed that the 16,000-lb wheel load (plus 30 percent impact load) can be placed anywhere on the slab, but that the effective tire width in the transverse direction is 20 in., so that only part of the wheel load is exerted on a given slab unit if the center of the wheel is placed less than 10 in. from the longitudinal joint. In computation of transverse bending moments in the concrete, it was conservatively assumed that there was neither shear nor moment transfer at the longitudinal joints. This assumption was made to simplify the slab design and to make sure that the slab

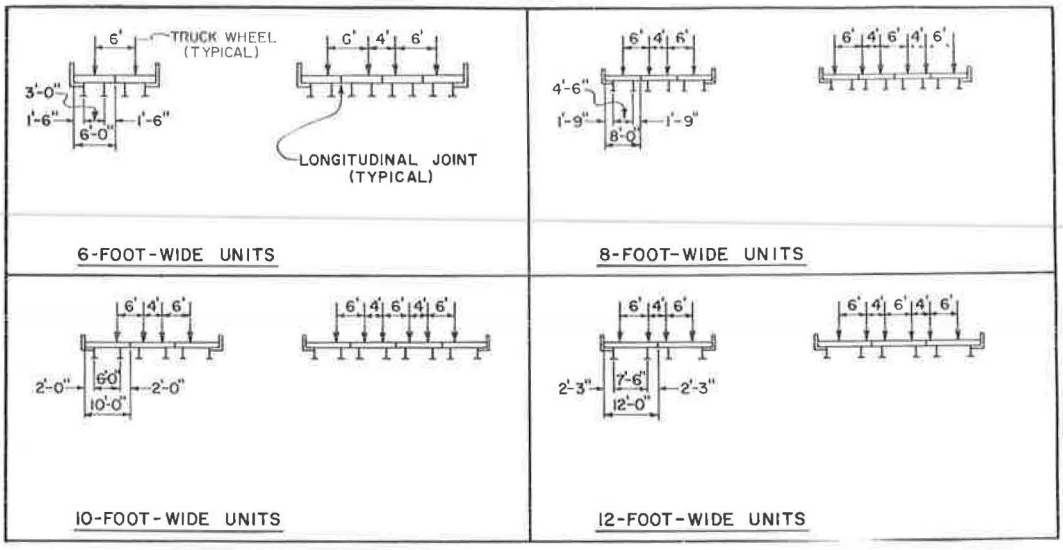

Figure 2. Typical bridge cross sections.

reinforcing steel would be adequate for any bridge assembly, even if the longitudinal joints were not keyed together. The vertical steel web plates, which support the deck slabs, were spaced so that the negative transverse bending moment (tension in top fibers of deck) in the slab at the steel webs would be equal to the maximum positive bending moment (tension in bottom fibers of deck) in the slab between webs and thereby allow the same top and bottom transverse reinforcement. Longitudinal reinforcement, which enables the slab to distribute wheel loads in the longitudinal direction, is specified by AASHO as a percentage of the transverse reinforcement.

On the basis of these considerations, the spacings of beam webs and reinforcing-bar requirements given in Table 1 were determined in accordance with the specifications. These beam-web spacings and reinforcing-bar requirements apply specifically to the prefabricated bridges. For shored cast-in-place bridges, it would be more logical to use equal spacing of tees, and the reinforcing-bar requirements would be less.

The possibility of longitudinal cracks occurring in the surface of the deck above the web of the T-beam due to the negative moment that occurs above the web was investigated experimentally in conjunction with T-beam punching shear tests (1) conducted at the U. S. Steel Applied Research Laboratory. In these tests, top surface cracking did not occur until a negative moment corresponding to a wheel load of about 40,000 lb—almost twice the wheel load for an HS20 truck plus impact—was applied. Thus, for static loading, top surface cracking probably would not be any more of a problem in the prefabricated units with inverted steel T-beams than in conventional composite bridges. To the author's knowledge, no fatigue tests have been conducted to determine whether problems of concrete cracking might occur in this type of construction under repeated loading.

Because about a 100-kip offset punching load was supported before failure, these T-beam punching shear tests indicated that, if the gaps between the bottom reinforcing bars and the steel webs are sufficiently small, the lap of the studs and the bottom reinforcing bars is sufficient to develop resistance to the small transverse positive bending moments that may occur in the slab directly over the web.

BEAM DESIGN

Live-Load Distribution Factors

The live-load bending moments in the longitudinal direction depend on the position of the truck wheels with respect to the beam in both the longitudinal and transverse

TABLE 1

BEAM-WEB SPACING AND SLAB REINFORCEMENT REQUIREMENTS

Width of Slab Unit (ft)	Spacing of Pair of Beam-Web Plates in Slab Unit (ft)	Distance from Beam-Web Plate to Longitudinal Joint (ft)	Transverse Reinforcing Steel[a]			Longitudinal Reinforcing Steel[a]		
			Size No.	Diameter (in.)	Top Bar Spacing and Bottom Bar Spacing (in.)	Size No.	Diameter (in.)	Top Bar Spacing and Bottom Bar Spacing (in.)
6.00	3.00	1.50	5	5/8	8	4	1/2	10
8.00	4.50	1.75	6	3/4	8	4	1/2	8
10.00	6.00	2.00	6	3/4	7	4	1/2	7 1/2
12.00	7.50	2.25	6	3/4	6	4	1/2	7 1/2

[a]Structural or intermediate grade.

directions. The longitudinal position resulting in maximum moment at a given location for any given span is easily calculated by conventional design procedures. However, once that is determined, it is necessary to determine what proportion of the truck wheel loads, and hence longitudinal moments, are supported by any given beam when the wheels are positioned transversely to cause maximum stress in that beam. (As used in this context, a beam consists of a single web, a steel flange, and the effective portion of the concrete slab acting with the single web.) The live-load distribution factor is the fraction of the moment of one longitudinal line of wheel loads (half of one truck, or half of one "lane" of loading equivalent to a single series of trucks on the span) that is carried by one beam when the bridge is loaded by trucks positioned to produce maximum moment in that beam.

An exact calculation of live-load distribution factors would be prohibitively complicated, since the load distribution depends on the stiffness of the steel T-beams, transverse diaphragms, and concrete slab acting as a composite unit. On the basis of in-service experience, AASHO specifies a live-load distribution factor equal to S/5.5 for steel-beam bridges with concrete decks, where S is the average spacing of beam webs measured in feet. It could be argued that this AASHO factor might be unconservative for bridges with longitudinal joints in the deck because the presence of the longitudinal joints might reduce the transverse stiffness of the deck. However, the rigidity of the joint detail provided by the clamping action of the transverse tie rods would tend to keep any reduction in transverse deck stiffness small. Furthermore, any reduction in deck stiffness could be counteracted by using more steel diaphragms between T-beams. Therefore, it appears that reasonable designs can be obtained by using the AASHO live-load distribution factor. Nevertheless, two sets of bridge designs are included in the present study: one based on the AASHO live-load distribution factor, and the other based on what will be called the "hinged-joint live-load distribution factor."

This second factor, which is computed from the equations given in Figure 3, is based on the hypothetical assumption that the diaphragms between tees have no bending stiffness and that the longitudinal joints have zero bending rigidity; that is, they act like frictionless hinges. The further conservative assumption is made that the beams are infinitely stiff compared with the stiffness of the slab, so that a load applied to the slab directly over a beam web would affect only that beam. Thus, the lateral distribution of load to other beams provided by the slab is neglected. The conservatism of neglecting lateral distribution is indicated by the fact that when the spacing of wheels given by AASHO is used, theoretical distribution factors based on equally spaced, infinitely stiff supporting beams (1.000, 1.200, 1.236, or 1.336 corresponding to beam spacings of 3, 4, 5, or 6 ft, respectively) would be considerably greater for conventional bridges than the S/5.5 specified by AASHO (0.545, 0.727, 0.909, or 1.091 corresponding to beam spacings of 3, 4, 5, or 6 ft, respectively).

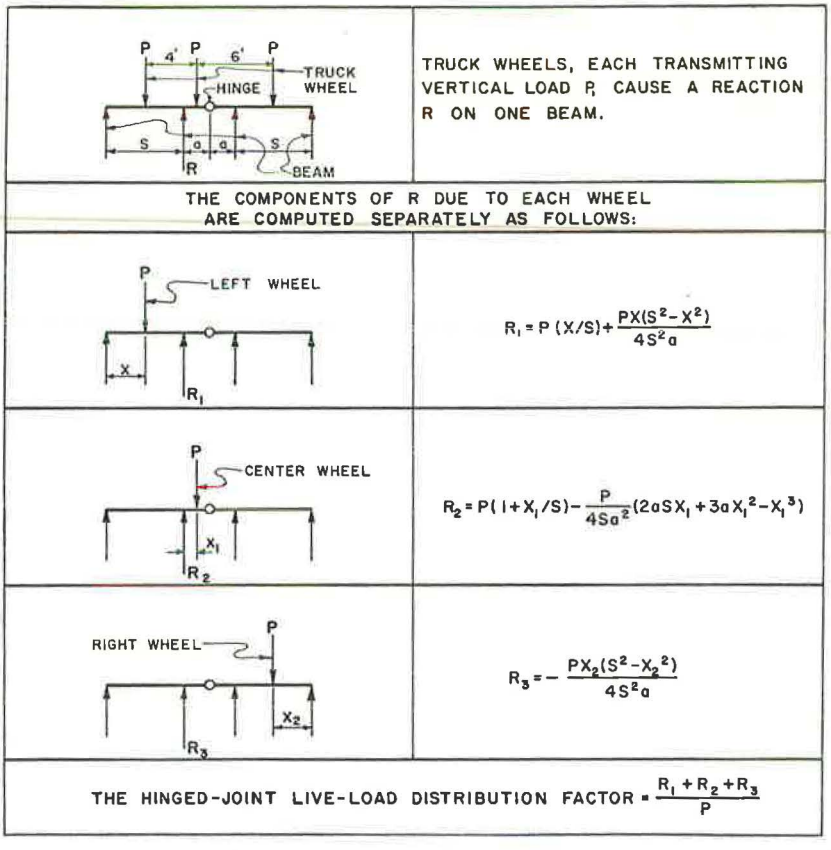

Figure 3. Loading diagrams and general formulas for hinged-joint live-load distribution factors.

For the different beam spacings of the present study, live-load distribution factors computed by the equations in Figure 3 were 1.000, 1.400, 1.390 (1.400 was used), and 1.532 for most critical position of loads on the 6-, 8-, 10-, and 12-ft wide units, respectively (Fig. 2). The rules about spacing of wheels given by AASHO were used to develop the hinged joint live-load distribution factors.

A different, less conservative assumption—that the stiffness of the transverse diaphragms causes all beams in a given bridge span to deflect the same amount—is allowed by AASHO for computing live-load deflections of bridges, and was also used for all deflection calculations of the present study. Most critical live-load distributions based on this assumption were 0.500, 0.750, 0.750, and 1.000 for the 6-, 8-, 10-, and 12-ft wide units, respectively (Fig. 2).

Calculations for Beam Main Material

Once the live-load distribution factors were determined, the beam requirements could be calculated by conventional bridge-design procedures. It was assumed that half of the concrete in each unit acted compositely with each steel T-beam. However, because of the many computations required for optimized solutions, a digital computer was used for calculations. Specifically, for a large number of different spans, several designs, differing only in the depth of the steel T-beams, were made for each of the eight cases: 6-, 8-, 10-, or 12-ft wide units with live-load bending moments determined by either the AASHO distribution factor or the hinged-joint distribution factor.

Although the designs with the hinged-joint distribution factors apply specifically to the prefabricated bridges, the designs with the AASHO factors apply both to the pre-

fabricated bridges, with beam spacing as shown in Figure 2, and to shored cast-in-place bridges with equal spacing of T-beams, with the 6-, 8-, 10-, and 12-ft wide designs applying to the cast-in-place bridges with 3-, 4-, 5-, and 6-ft tee spacings, respectively.

The data from these calculations, which should be useful to designers for estimating weight, selecting beam depths corresponding to minimum weight, and determining bottom-flange area required, are indicated as curves in Figures 4 through 11, one case being summarized in each figure. In these figures, the bottom flange areas and weights of the steel T-beams per square foot of deck area were plotted individually as functions of span length. The weights in these charts do not include the weights of the A36 steel diaphragms, about 2 to 3 psf, or the A36 steel beam stiffeners, about 2 to 7 psf. Any combination of flange thickness and width that does not violate the maximum width-to-thickness ratio of 12 stated in the specification for outstanding legs of flanges could be used to provide the required area, but if the thickness exceeds $^3/_4$ in., an increase in area is required, as discussed next. All designs are based on a steel allowable bending stress of 27,000 psi—the specification allowable stress for high strength A441 or A242 steel $^3/_4$ in. or less in thickness. If a plate thicker than $^3/_4$ in. is used, the required area of the plate must be increased by a factor slightly greater than 1.125, since the specification allowable stress for high-strength A441 or A242 steels in thicknesses exceeding $^3/_4$ in. but not $1^1/_2$ in. is 24,000 psi. This reduction in the allowable stress corresponds to the reduction of the specified minimum yield point of A441 or A242 steels from 50,000 to 46,000 psi when thicknesses exceed $^3/_4$ in. Alternatively, certain proprietary A441 (modified) steels that maintain a specified minimum yield point of 50,000 psi for considerably greater thicknesses could be used for flanges thicker than $^3/_4$ in. without increasing the area requirements.

Although bending moments are usually the most important considerations in determining the requirements for beam main material, shear forces sometimes set minimum thickness requirements for the webs. All webs in this study were stressed in shear well below the specification allowable value of 15,000 psi, and all meet the requirement for webs stiffened with transverse stiffeners, that the web thickness be not less than $^1/_{140}$ times the clear depth of the web, defined as the depth between the bottom of the deck slab and the top of the bottom flange plate. Where, in this study, the depth of the web exceeds about $15^1/_2$ in., i.e., 50 times the thickness for steel with a 50,000-psi yield point, the web must be stiffened with transverse intermediate stiffeners in accordance with Section 1.6.80 of the AASHO specification to prevent shear buckling of the webs.

Design of Studs Connecting Steel Webs to Concrete Decks

The spacing of the steel studs which connect the tops of the web plates to the concrete deck slabs should be determined in accordance with Section 1.9.5 of the AASHO specifications, with the modification that the calculated shearing forces on the studs should be the vector sum of: (a) the horizontal shear from composite action, computed by conventional procedures, and (b) the localized vertical punching shear that would be caused by a truck wheel offset horizontally a slight amount from the plane of the steel web. This vertical punching shear is not described in the AASHO specifications and is not important in conventional beams with top flanges because the stud connectors on such beams are generally vertical and therefore only have to resist the horizontal shear from composite action. To determine approximately what intensity of vertical punching shear should be considered in the stud designs of this study the Applied Research Laboratory performed punching tests on two composite specimens, each consisting of a 7-in. thick reinforced-concrete slab 10 ft wide by $5^1/_2$ ft long cast with two vertical steel webs 6 ft apart. (The punching shear carried by each stud cannot be determined analytically because the longitudinal distribution of the wheel loading and the percentage of the total punching shear that is carried directly by the web are not known.) Thus, the specimens represent a section of a composite bridge with 10-ft wide deck units (Fig. 2). As a result of these tests, it was suggested that the maximum vertical punching shear per stud, due to dead load and HS20 live load and impact, be $342S$ lb, where S is the spacing of studs on one side of the web in inches. Studs should

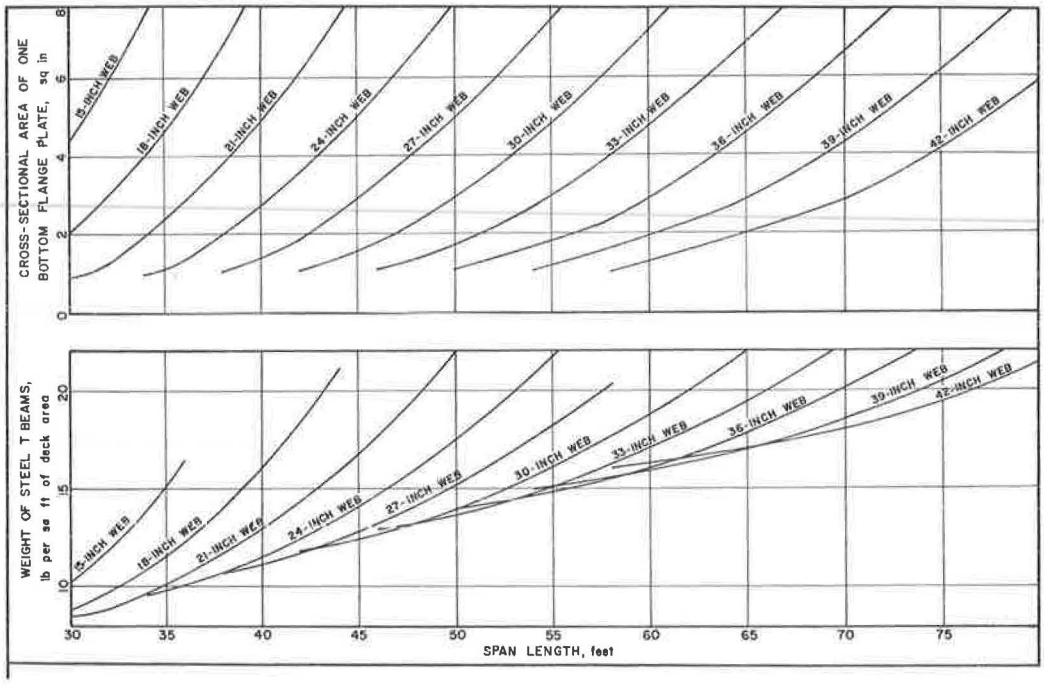

Figure 4. Six-ft wide composite bridge unit with two inverted T-beams, based on AASHO live-load distribution factor.

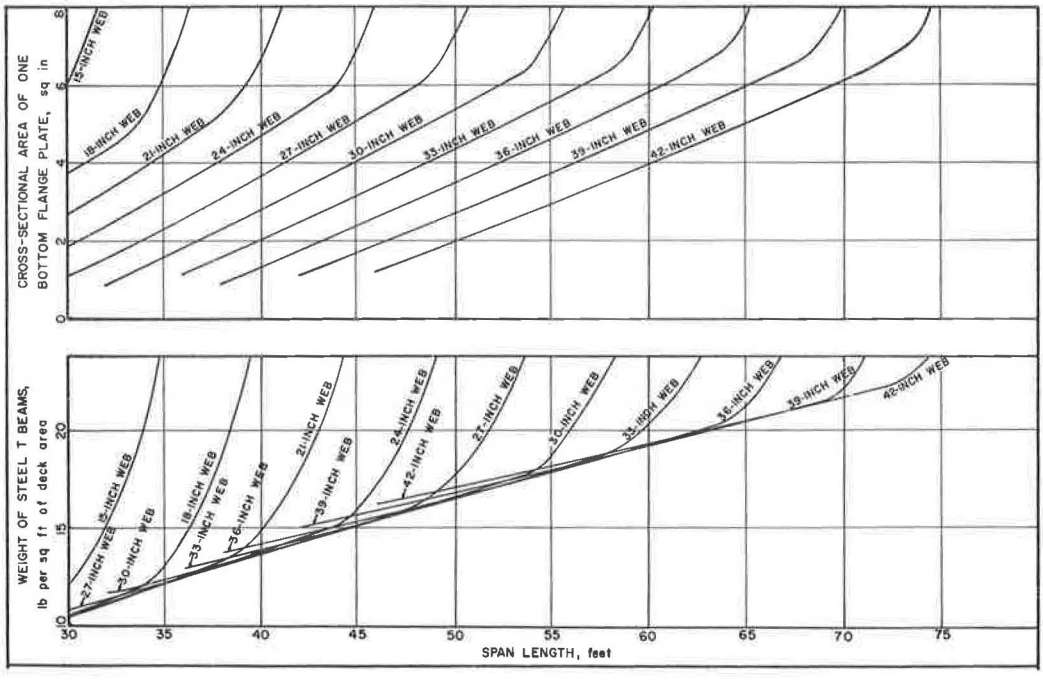

Figure 5. Six-ft wide composite bridge unit with two inverted T-beams, based on hinged-joint live-load distribution factor.

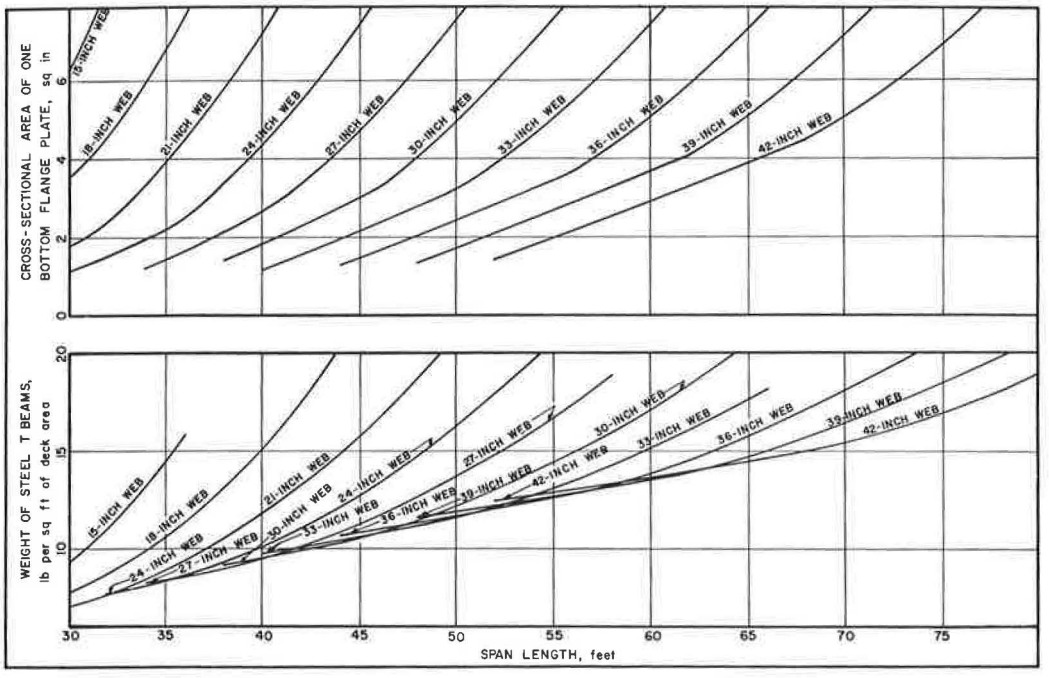

Figure 6. Eight-ft wide composite bridge unit with two inverted T-beams, based on AASHO live-load distribution factor.

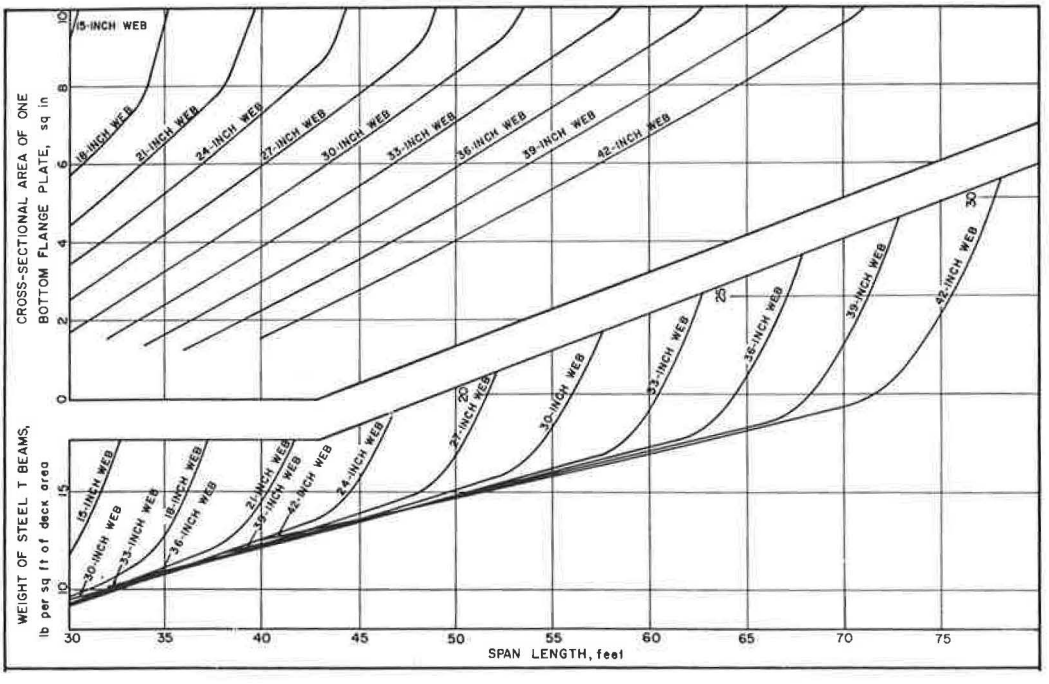

Figure 7. Eight-ft wide composite bridge unit with two inverted T-beams, based on hinged-joint live-load distribution factor.

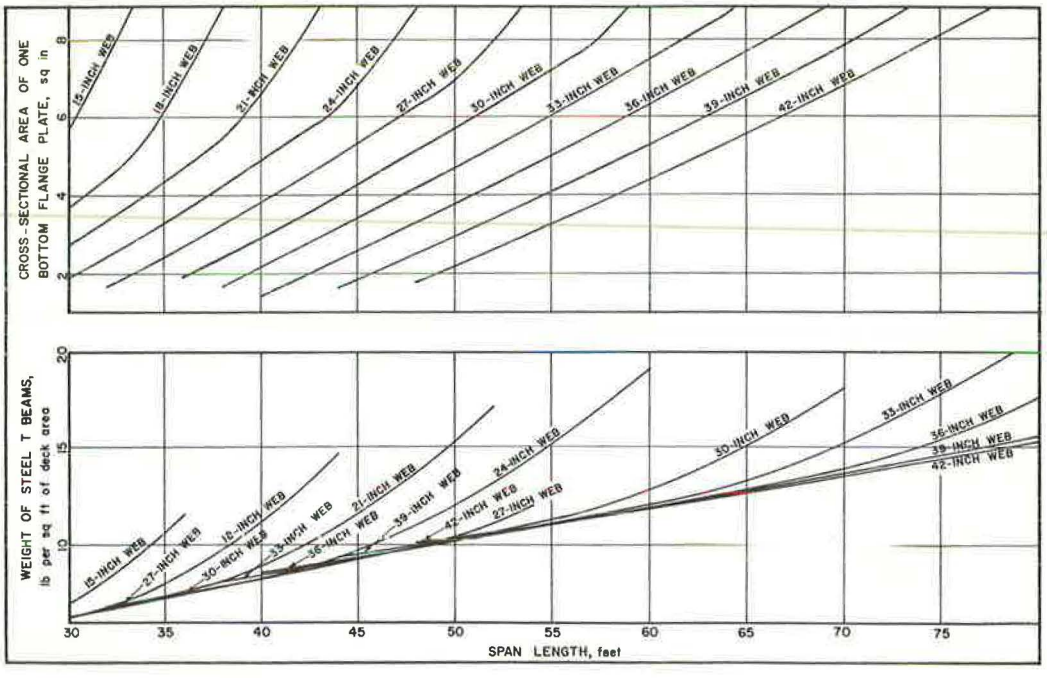

Figure 8. Ten-ft wide composite bridge unit with two inverted T-beams, based on AASHO live-load distribution factor.

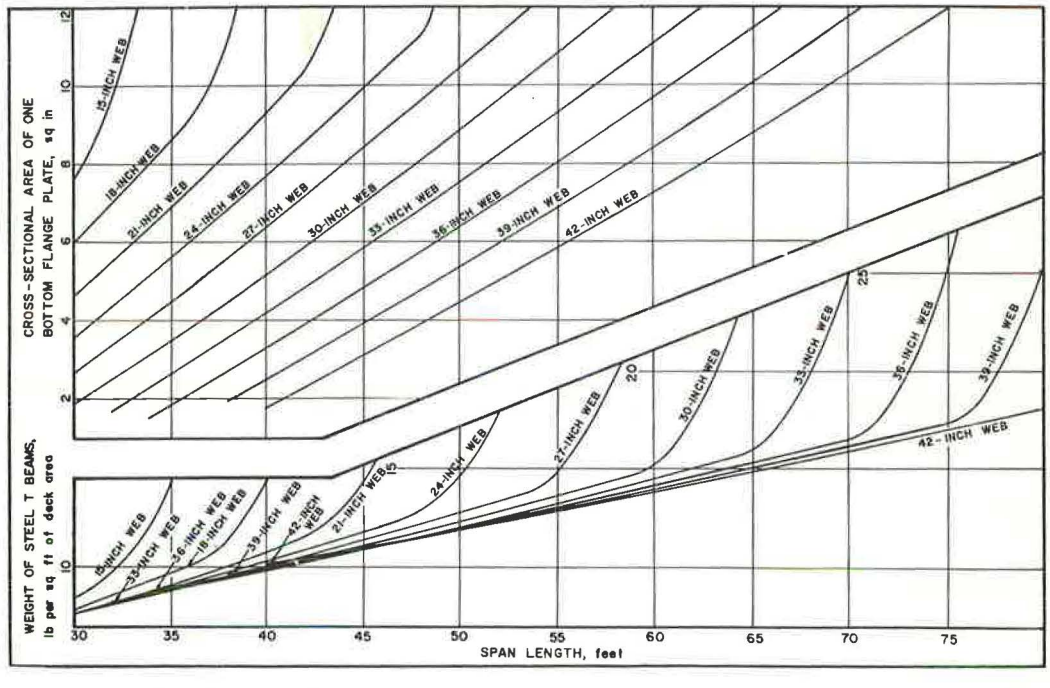

Figure 9. Ten-ft wide composite bridge unit with two inverted T-beams, based on hinged-joint live-load distribution factor.

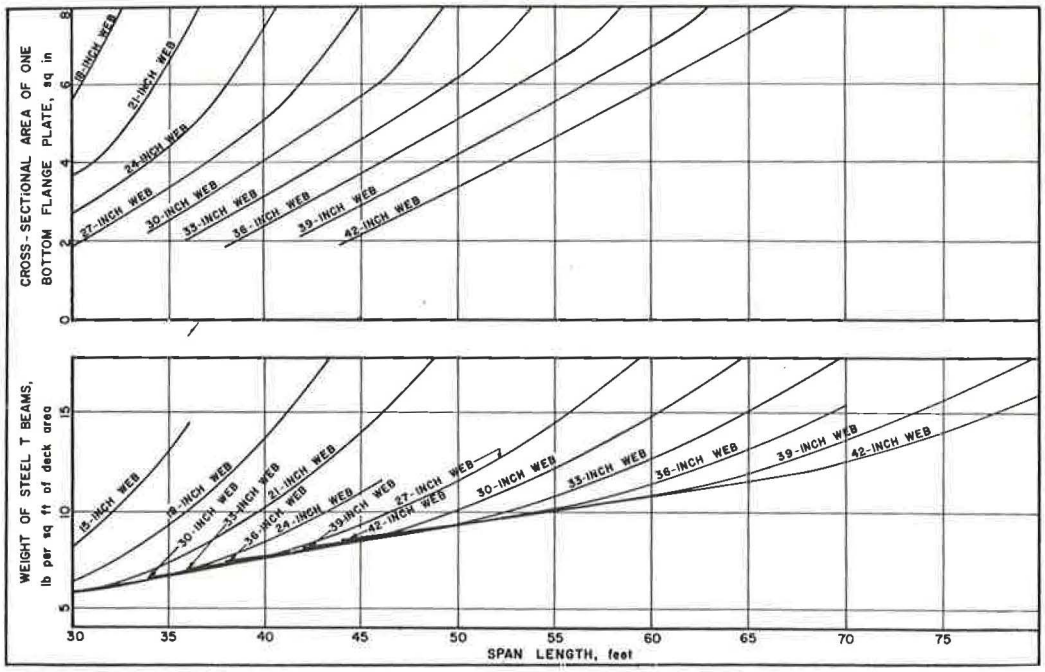

Figure 10. Twelve-ft wide composite bridge unit with two inverted T-beams, based on AASHO live-load distribution factor.

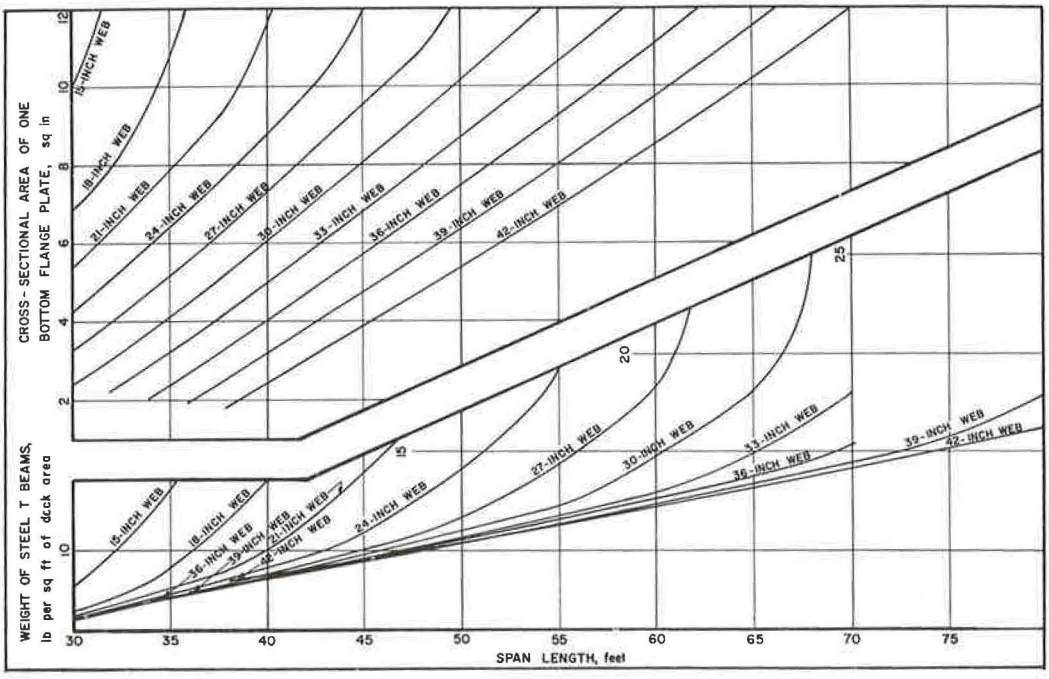

Figure 11. Twelve-ft wide composite bridge unit with two inverted T-beams, based on hinged-joint live-load distribution factor.

be equally spaced on both sides of the web, and to minimize the possibility of the web warping, they should be placed directly opposite each other. Because the punching-shear formula was derived from tests on a 10-ft wide configuration, it can also be applied conservatively to the 8-ft wide and 6-ft wide configurations. Also, since the total live-load punching shear for the 7½-ft web spacing of the 12-ft wide bridge units is theoretically only about 3 percent greater than the total live-load punching shear for the 6-ft web spacing of the tests, it also appears satisfactory to apply the formula to bridges with the 12-ft wide configuration.

To determine whether ¾-in. diameter studs could be used in the present designs without objectionable crowding, stud-spacing calculations were made for 16 typical bridge designs with spans ranging from 40 to 70 ft and with span-to-web depth ratios ranging from about 18 to 20. Specifically, the maximum allowable spacing at the end of span was calculated for ¾-in. diameter by 4-in. long steel studs that have an ultimate shearing strength of 11,000 lb per connector when embedded in concrete with an ultimate compressive strength of 3,500 psi. The calculated stud spacing on each side of the web ranged from about 5.2 in. for a 6-ft wide unit to about 3.2 in. for a 12-ft wide unit. Thus, it appears that the use of ¾-in. diameter studs would not generally result in objectionable crowding of studs, but that the use of smaller diameter studs, which have less strength, would probably result in an undesirably close spacing.

For a particular bridge, the most efficient stud spacing, which may vary by steps along the length of the bridge, can best be selected by the designer. Therefore, stud spacings are not given herein.

DESIGN OF BRACING BETWEEN BEAMS

To help distribute live loads and to resist racking from wind and other causes, the AASHO specifications require that in beam or girder bridges intermediate transverse bracing between adjacent beams or girders be placed at longitudinal intervals not exceeding 25 ft. However, the strength and stiffness requirements for the bracing are not specified and cannot readily be calculated. Therefore, the design of such bracing is based on engineering judgment or "rule-of-thumb" methods. In composite beam bridges of the span range considered here, a diaphragm consisting of a steel channel is usually used as the bracing.

To insure adequate live-load distribution so that the AASHO distribution factor may be confidently used for the present designs in spite of the existence of the slab longitudinal joints between adjacent units, it would be desirable to provide more transverse stiffness than is usually provided. This could be accomplished by using X bracing or stiff beam diaphragms and/or reducing the spacing of the bracing. As in conventional designs, however, the exact selection of the bracing must be left to the individual designer's judgment, because the bracing requirements are too complex to be readily calculated.

The end diaphragms, however, support the wheel loads positioned on the deck in the vicinity of the end bearings of the beams, and do not affect the apparent rigidity of the longitudinal joints. Therefore, the end diaphragms should consist of rolled beams, designed to support a 16,000-lb vertical wheel load, plus 30 percent for impact.

PREFABRICATED COMPOSITE BRIDGES WITH INVERTED STEEL T-BEAMS VS PRESTRESSED CONCRETE BOX-BEAM BRIDGES

In 1963, four members of the Indiana Steel Fabricators Association prepared detailed cost estimates for fabrication at plant, not delivered to site, of a 50-ft bridge consisting of one 10-ft wide and two 8-ft wide prefabricated composite units with inverted steel T-beams. On top, a 24-ft wide roadway is flanked by two 1-ft wide escape walks with post-and-guardrail railing attached. Each prefabricated unit has a pair of 33- by 5/16-in. A441 steel webs, and the A441 steel bottom flanges are 9½ by ½ in. in the 10-ft wide unit and 6½ by ½ in. in the 8-ft wide units. A total of 156 ¾-in. diameter by 4-in. long steel studs is welded to each web of the 10-ft wide unit, and 128 studs are welded to each web of each 8-ft wide unit. Intermediate diaphragms between beam webs, which are spaced at 10-ft intervals in the longitudinal direction,

TABLE 2

ESTIMATED COSTS OF 50-FT LONG PREFABRICATED COMPOSITE BRIDGE MADE WITH INVERTED STEEL T-BEAMS

Fabricator Identifying Letter[a]	Cost of Units ($ per sq ft of bridge deck)		
	Structural Steel[b]	Reinforced Concrete	Total for Finished Unit[c]
A	3.62[d]	1.77	5.39
B	3.62	2.04	5.66
D	5.40	2.04	7.44
E	2.96	1.58	4.54
Avg.	3.90	1.86	5.76

[a] In Indiana Steel Fabricators Assoc. correspondence.
[b] Including beams, studs, stiffeners, bracing, railing, and tie rods.
[c] Ready to be shipped from fabrication plant.
[d] Fabricator A did not include the cost of guardrail. The other fabricators did include the cost of guardrail.

are X bracings consisting of A36 steel single angles 4 by 3 by $\frac{5}{16}$ in., and the transverse diaphragms at the end of the span are A36 steel channels weighing about 20 lb per foot. The design loading was HS20, and the AASHO live-load distribution factors were used in the design. The fabricators' detailed estimates for this bridge are given in Table 2.

An August 1963 survey of three major Michigan producers of concrete products indicated that the cost of 27-in. deep prestressed concrete box beams adequate to span 50 ft under HS20 loading, delivered to a job site but not erected, was currently about $6.25/sq ft of bridge deck. However, it was not possible to determine the cost at the fabrication plant, because the producers usually absorb freight charges and sell directly to contractors at job sites. Nevertheless, one of the producers stated that throughout continental United States the cost at the fabrication plant of 27-in. deep prestressed concrete box beams capable of spanning 50 ft, figured as selling price minus freight cost, is probably between about $4.25 and $5.75/sq ft of bridge deck. On the basis of about $0.50/sq ft for railing, the cost at the fabrication plant would be between about $4.75 and $6.25/sq ft for the prestressed concrete box beams. These costs compare closely with the fabricators' estimates indicated in Table 2. Therefore, it appears that prefabricated composite bridge units with inverted steel T-beams would be competitive with prestressed concrete bridges.

CONCLUSION

It thus appears that prefabricated composite highway bridge units with inverted steel T-beams would be both structurally adequate and economical. However, to demonstrate the performance of these prefabricated bridges and to determine experimentally the appropriate live-load distribution factors, it would be desirable to build and test a prototype bridge.

ACKNOWLEDGMENT

Appreciation is extended to the Indiana Steel Fabricators Association for furnishing the cost estimates for the hypothetical bridge.

REFERENCE

1. McDermott, J. F. Tests Evaluating Punching Shear Resistance of Prefabricated Composite Bridge Units Made with Inverted Steel T-Beams. Highway Research Record 103, pp. 41-52, 1965.

Dynamic Studies on the Bearing Capacity of Piles

G. G. GOBLE, R. H. SCANLAN and J. J. TOMKO
Respectively, Associate Professor, Professor and Graduate Assistant, Case Institute of Technology, Cleveland, Ohio

ABRIDGMENT

•THE general philosophy behind this study is that information is generated during driving which can yield a measure of the static bearing capacity. Until recently, due to high frequency dynamic effects generated by the driving operation, permanent set was the only measurement which could be made reliably. This limitation led to the use of the energy approach upon which the numerous pile formulas are based.

Developments in electronic instrumentation and transducers in the past few years make it possible to consider making routine acceleration, velocity and force measurements on piles during driving.

A single force-balance theory is proposed to relate dynamic measurements to static capacity. This theory has sufficient simplicity for use on a routine basis. It assumes the pile to be a rigid body struck by a time-varying hammer force. Motion of the pile is resisted by a force, R, given by a series

$$R(t) = R_0 + R_1 v + R_2 v^2 + R_3 v^3 + \ldots$$

where v is the velocity of the pile and R_0, R_1, R_2, etc., are constants (Poncelet's Law). R_0 represents the static bearing capacity. If the pile is examined under the action of these forces with Newton's equation the resistance is found to be

$$R_0 = F(t_0) - m\, a(t_0)$$

where m is the mass of the pile, a(t) is the acceleration and t_0 is the time when v = 0. Therefore, it is necessary to measure F(t) and a(t).

Equipment was assembled to make the necessary measurements. Accelerations were measured a short distance below the top of the pile using a piezoelectric accelerometer. Force measurements were made with resistance strain gages attached directly to the pile. A continuous record of force and acceleration was obtained on a high-speed oscillograph.

Data were collected from two different sources. Small-scale piles were driven using an apparatus constructed for that purpose. In addition, records were obtained from full-scale test piles driven and load tested in connection with Ohio Highway Department construction projects.

The small-scale piles were made of 2½-in. diameter steel pipe. They were driven to depths of up to 20 ft in a medium-coarse, well-graded sand. Static pile capacities were measured by both rapid and slow load tests. The results of the tests are given in Table 1. It was observed that much better correlation was obtained if the pile was re-driven after performance of the static load test. Thus, the effect of "set up" of the pile was obtained. The proposed theory predicts ultimate capacity. Consequently, when the load test was not carried to ultimate but was stopped at some predefined slope of the load displacement curve, it was necessary to extrapolate the curve upward to

Paper sponsored by Committee on Substructures, Retaining Walls and Foundations and presented at the 46th Annual Meeting.

TABLE 1

EXPERIMENTAL RESULTS

Pile	Soil Type	Results at End of Driving		Results After "Set up" Period		
		Rapid Test (kips)	Dynamic Prediction (kips)	Rapid Test (kips)	Slow Test (kips)	Dynamic Prediction (kips)
Model 13-1	Sand			8.86	8.65	5.32
Model 15-1	Sand			11.4		9.91
Model 15-2	Sand		10.39	12.9	12.7	
Model 15-3	Sand	14.8	13.0	18.3		20.66
Model 15-4	Sand		9.71	10.6		11.31
Model 15-6	Sand		9.71	12.1		13.54
Model 15-7	Sand		9.94	14.0		16.49
Full-scale 138	Silt and clay		119	270.0	260-300	
Full-scale 113	Sand		244		200-240	
Full-scale 103	Sandy silt				196-220	222
Full-scale A	Sandy silt			252	230-280	281

ultimate. The proposed theory was applied to the results of studies conducted in Michigan (1). The results are given in Table 2.

Based on the results from this project and the Michigan tests, the correlation with the proposed simplified theory is very promising. Further tests are necessary in a variety of soil types. Full-scale tests are particularly important and useful. Any method of prediction of static capacity based on measurements obtained during driving can be expected to predict the capacity at the time of measurement. Estimates of strength gain must be based on soil studies. The use of the system described here in connection with re-driving appears to provide an accurate strength measure.

The wide variety of ultimate load capacities measured on the model piles is disturbing to the concept of the single-load test pile. These piles were quite closely spaced but their capacities differed rather widely. The use of the system proposed here would make practical the dynamic testing of many piles.

REFERENCE

1. A Performance Investigation of Pile Driving Hammers and Piles. Michigan State Highway Commission, Lansing, March 1965.

TABLE 2

PROPOSED THEORY APPLIED TO MICHIGAN RESULTS

Pile Designation	Soil Condition	Load Test Capacity[a] (tons)	Proposed Theory Capacity[b] (tons)
Belleville			
LTP-1	Clay	120	107
LTP-3	Clay-tip in very fine sand and silt	210	58.9
LTP-6	Clay-tip in very fine sand and silt	250	197
Detroit			
LTP-1	Clay	32.5	22.7
LTP-2	Clay	53.6	59.7
LTP-7	Clay	190	58.3
LTP-8	Clay	250	52.6
Muskegon			
LTP-2	Sand	125	115
LTP-3	Sand	75	71.7
LTP-9	3 Layers loose sand soft sed's peat compact sand	290	193

[a]This value is obtained from extrapolation of the load-settlement curve given for each pile. The value given is the plastic failure load.

[b]Load obtained from considering both pile wt and plain driving cap and cushion assembly.